

Article

Effect of the Freezing Step on Primary Drying Experiments and Simulation of Lyophilization Processes

Alex Juckers ^{1,2} , Petra Knerr ², Frank Harms ² and Jochen Strube ^{1,*}

¹ Institute for Separation and Process Technology, Clausthal University of Technology, 38678 Clausthal-Zellerfeld, Germany

² Martin Christ Gefriertrocknungsanlagen GmbH, 37520 Osterode am Harz, Germany

* Correspondence: strube@itv.tu-clausthal.de

Abstract: Lyophilization is a widely used preservation method for thermosensitive products. It consists of three process steps: freezing, primary and secondary drying. One of the major drawbacks is the long processing time. The main optimization effort was put into the primary drying phase since it is usually the longest phase. However, the freezing step is of immense importance for process efficiency and product quality. The lack of control during freezing comprises a challenge for process design and tech transfer. In this study, four different freezing steps (shelf-ramped freezing with and without holding step, precooled shelves and an ice fog method for controlled nucleation) are used and their impact on primary drying experiments and simulations is shown. Only the ice fog method is able to control the nucleation temperature leading to low dry layer resistances with low deviations. During the primary drying simulations, the control of the nucleation temperature drastically increases the precision and accuracy of the product temperature prediction. For optimal primary drying design and model predictive control, the nucleation temperature is strongly recommended to be controlled inside a Process Analytical Technology (PAT) concept to achieve reliable and reproducible process conditions.

Keywords: lyophilization; controlled nucleation; Process Analytical Technology (PAT); Quality by Design (QbD); process modelling; advanced process control (APC)



Citation: Juckers, A.; Knerr, P.; Harms, F.; Strube, J. Effect of the Freezing Step on Primary Drying Experiments and Simulation of Lyophilization Processes. *Processes* **2023**, *11*, 1404. <https://doi.org/10.3390/pr11051404>

Academic Editor: Jean-Louis Lanoiselle

Received: 27 March 2023

Revised: 28 April 2023

Accepted: 2 May 2023

Published: 5 May 2023



Copyright: © 2023 by the authors. Licensee MDPI, Basel, Switzerland. This article is an open access article distributed under the terms and conditions of the Creative Commons Attribution (CC BY) license (<https://creativecommons.org/licenses/by/4.0/>).

1. Introduction

Freeze-drying or lyophilization is the gold standard of drying and is particularly suitable for thermosensitive pharmaceutical products such as proteins and vaccines [1]. It is estimated that 60% of all biologic products would not be available without freeze-drying, as this process significantly improves the shelf life [2]. In fact, 16% of the TOP100 medicines and 35% of all biotechnologically produced medicines are freeze-dried [3]. In solid form, the active drug is immobilized, inhibiting or significantly reducing chemical and physical degradation [4,5]. Solid-form active drugs offer many advantages including easy handling and storage as well as lower transportation costs, but they are not as easy to manage as ready-to-use solutions [6,7]. Lyophilization consists of three steps: freezing, primary and secondary drying. During the freezing step, liquid water is transformed into solid ice. The primary drying phase removes the ice by sublimation under vacuum and the secondary drying establishes the final residual moisture of the product. Traditionally, freeze-drying processes are developed on the basis of trial and error and empirical values, followed by validation of a process that is not changed throughout the entire product life cycle and involves high safety margins [4,8]. The growing number of biotechnologically produced molecules will result in an increased demand for freeze-drying equipment and processes [9]. Here, a paradigm shift in process development is necessary, away from purely empirical methods towards regulatory required methods that develop the process based on risk assessment and process understanding [10–12].

The freezing step is of the utmost importance and influences the product morphology and the ice crystal size and form, thus influencing the drying performance. Furthermore, it is critical for product stability, and the average ice crystal size determines the quality of the final product [13]. A change in ice crystal size can lead to cold unfolding or denaturation, modification of the environment (change in pH, ionic strength, phase separation and composition) and denaturation by ice crystals, causing product degradation [14,15]. Non-systematic selection of freezing conditions leads to a weak control strategy [13,16]. During conventional freezing methods, the nucleation temperature and time cannot be controlled, which is contrary to the Quality by Design (QbD) principle wherein Process Analytical Technology (PAT) is a crucial part in the achievement of process understanding and control to achieve improved product quality (see Figure 1).

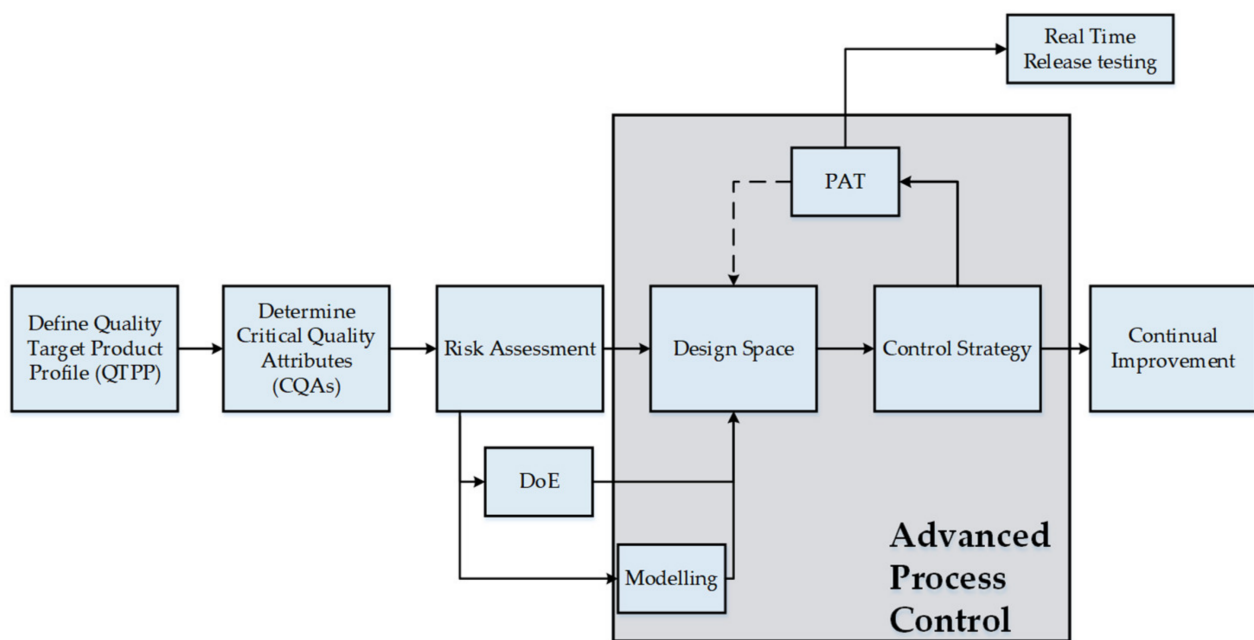


Figure 1. QbD process development workflow [17].

In this work, the influence of the freezing method on the nucleation temperature, dry layer resistance, heat flux data and primary drying performance is compared. Additionally, the influence of the freezing method on primary drying simulation is evaluated. The control of the nucleation temperature leads to a lower dry layer resistance with smaller deviations. The simulation results increase in accuracy and precision with the use of controlled nucleation. It is shown that the control of the nucleation temperature is critical to decrease the variability of the freeze-dried product. For optimal primary drying simulation, aggressive primary drying conditions should be combined with controlled nucleation. The usage of controlled nucleation reduces intra- and inter-vial heterogeneity and can simplify scale-up and process development and should therefore be incorporated into an Advanced Process Control (APC) concept.

2. Freezing Fundamentals

The freezing step is the major dehydration step in lyophilization [18] and the most complex and important step during lyophilization [19]. It consists of three stages:

- Cooling—liquid formulation is cooled to freezing temperature;
- Nucleation—the first ice nucleus is formed;
- Solidification—ice crystals grow until no water is available.

The corresponding product temperature during the freezing phase is shown in Figure 2. The sample is first cooled down; as soon as nucleation appears, the phase change leads

to a product temperature increase, which slowly decreases during crystallization and subsequently decreases as soon as all available water is frozen.

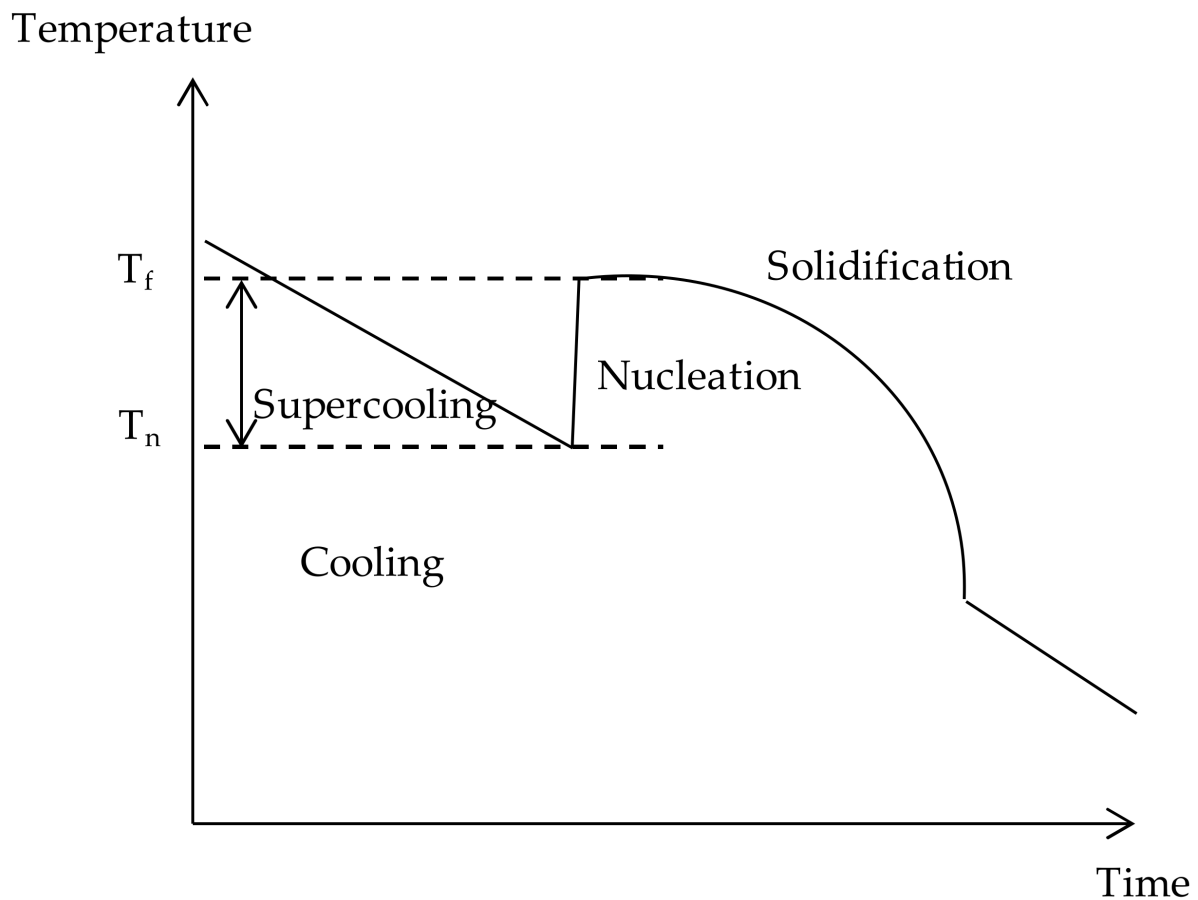


Figure 2. Product temperature during the different freezing events (illustration adopted from [20,21]).

2.1. Cooling

In the cooling stage, the temperature of the liquid formulation is lowered from the initial value to the nucleation temperature T_n . An aqueous solution does not freeze spontaneously at its equilibrium freezing temperature T_f at atmospheric pressure [22,23]. The maintenance of the liquid state below the equilibrium freezing point of the solution is called “supercooling”. It is defined as the difference between nucleation and the equilibrium freezing temperature [24] and lies inside a range of 10 to 15 K [25,26]. The degree of supercooling depends on the solution properties, process conditions and manufacturing environment [27]. It is a metastable state in which water molecules form ice-like clusters [28]. These clusters break up rapidly until an adequate quantity of molecules forms a stable aggregate, the critical nucleus. It provides suitable surfaces for ice crystal growth [27] and ice crystallization subsequently occurs rapidly [29,30]. Homogenous nucleation of water appears around -40 °C [5]; however, in pharmaceutical solutions, heterogenous nucleation is observed. Ice-like clusters form on impurities such as particulate contaminants [18,31–33]. Ice nucleation shows a random and stochastic nature, leading to ice crystal distributions that differ from vial to vial, inside the vial and from batch to batch, leading to deviations in drying behavior [34–36].

2.2. Nucleation

Once the product solution reaches the nucleation temperature, phase change begins. Ice crystal formation is an exothermic process. The supercooled solution is only able to absorb a limited amount of heat [26,30], leading to a product temperature increase to the equilibrium freezing temperature [37]. The absorbed amount of heat determines

the number of formed ice crystals and is controlled by the degree of supercooling [7]. Bigger amounts of heat can be absorbed by a higher degree of supercooling, leading to the formation of many ice crystals. Supercooling controls the number and size of the ice crystals and the ice growth rate [24,34]. Three different ice crystal morphologies can be observed [28,38]:

- Needle-like crystals: random arrangement of water molecules around ice nuclei with a high degree of supercooling;
- Regular hexagonal crystals (dendrites): ordered arrangement of water molecules around ice nucleus with low degree of supercooling;
- Ice spears (spherulites): spherulites form from the center of crystallization with high cooling rates.

2.3. Solidification

Ice crystals grow by the addition of remaining water to the interface of ice nuclei. Solutes cannot fit into the dense ice structure as it forms [31]. The solute concentration in the interstitial region is increased by the ice crystal growth leading to freeze concentration [5,26]. The overall solute concentration only depends on the temperature and is independent of the initial concentration [5]. Continued freezing increases the solute concentration to a critical value above which eutectic freezing or vitrification of the solution will occur [39].

Eutectic mixtures are formed by the crystallization of solutes from the concentrated solution [22]. The lowest temperature where the solution remains liquid is the eutectic temperature. Here, the freeze concentrate is saturated and the solute crystallizes [22,39]. Only below this temperature is the system completely solidified [22].

Amorph solutions vitrificate during freezing because of their complex microstructure [5]. Water freezes beyond the eutectic temperature, and as the solution becomes more saturated, the viscosity increases, slowing down ice crystallization until freezing stops. This phenomenon is called glassification or vitrification [25,40], and the corresponding temperature is called the glass transition temperature [41]. This temperature marks the point between a viscous liquid and a rigid glass. The glass consists of concentrated solutes and unfrozen water. The high viscosity limits the movement to a few millimeters per year [41].

The different states during the freezing step can be seen in the phase diagram of water and solute, shown in Figure 3. The unsaturated liquid solution is cooled down until nucleation occurs. Ice crystals form and the solution becomes cryo-concentrated. The system follows the equilibrium freezing curve as water is removed by ice crystal growth. At the eutectic temperature, the equilibrium freezing curve intersects the equilibrium solubility curve, leading to saturation of the freeze concentrate and subsequently eutectic freezing or solute concentration. Amorph solutes do not crystallize at the eutectic temperature. The freeze concentration continues and the solution becomes increasingly viscous until the equilibrium freezing curve intersects with the glass transition curve. Here, vitrification or glassification of the solutes occurs at the glass transition temperature.

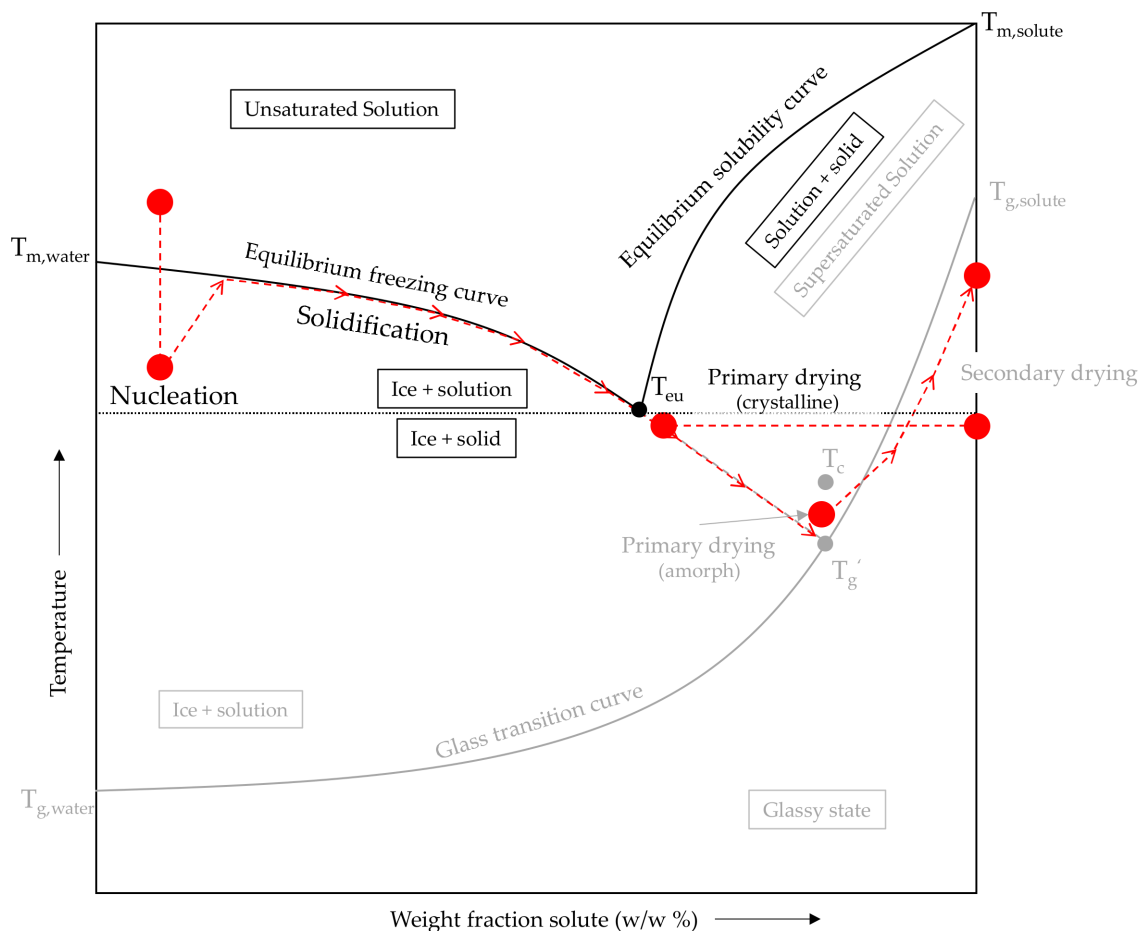


Figure 3. Phase diagram water/solute system (crystalline excipient: black, amorph: grey (illustration adopted from [7,23,42])).

The major difference between eutectic crystallization and vitrification is the composition of the interstitial area between the ice crystals. In amorphous solutions, it contains solid solution and unfrozen water, whereas in a crystalline substance, it contains only solute crystals [31]. Here, all water is frozen while amorphous substances can have about 20% unfrozen water [22]. Crystalline material only needs a primary drying phase to remove the frozen water while amorphous solutes require secondary drying to remove the unfrozen water from the solid. During primary drying, the eutectic melting temperature of a crystalline solution—and for amorphous solutes, the collapse temperature—is the maximum allowed product temperature. The collapse temperature is higher than the glass transition temperature since the high viscosity prevents flow. Exceeding the maximum allowed product temperature leads to structural loss of the dried product by meltback (crystalline) or collapse (amorph). The eutectic and glass transition temperature can be determined by (modulated) differential scanning calorimetry and differential thermal analysis [43–48] while the collapse temperature is determined by a freeze-drying microscope [49–52].

3. Freezing Methods and Effects on Process Performance

Different methods are available to freeze the solution during freeze-drying. They are summarized in Table 1. For a detailed description of every method, the authors recommend the following research [7,23,53]. Low supercooling leads to some big ice crystals, which increase the primary drying rate but decrease the secondary drying rate. In order to find the optimal process performance for the used formulation, a balance between these two rates has to be found.

Table 1. Summary of freezing methods and their impact on T_n and drying rates (CN: controlled nucleation, SSA: specific surface area, GMP: Good Manufacturing Practice, +++/---: extremely high/low, ++/--: very high/low, +/−: high/low, ✓: compatible, x: incompatible, n.i.: no indication, adopted from [23]).

Freezing Method	Procedure	CN?	T_n	SSA	R_p	Primary Drying Time	Secondary Drying Time	Integration (Equipment Change Necessary?)	GMP	Comments
Shelf-ramped freezing	Linear decrease in shelf temperature	No	--	++	++	++	--	No	✓	Most common used
Shelf-ramped step freezing	Linear decrease in shelf temperature with equilibration holding steps (e.g., 5 °C and −10 °C)	No	−	+	+	+	−	No	✓	Equilibration reduces the inter-vial heterogeneity
Pre-cooled shelf method	Vials are loaded onto shelf at desired temperature (e.g., −45 °C)	No	+	−	−	−	+	No	✓	High inter-vial heterogeneity, primary drying time reduction of up to 18%
Annealing	Holding step above glass transition temperature	No	n.i..	---	---	---	++	No	✓	Eliminates dependence of ice crystal size on nucleation temperature, reduces inter-vial heterogeneity,
Quench freezing	Immersion into liquid nitrogen or other solutions	No	+	+++	+++	+++	—	No	x	Lowered degree of supercooling, high freezing rate
Vertical freezing	Nucleation with dry ice at vial bottom	No	+	---	---	---	++	No	x	Produces large vertical ice crystals
Ice fog technique	Ice fog introduced into chamber, generated small ice crystals serve as nucleating agents	Yes	++	---	---	---	++	Yes	✓	Reduced pressure inside chamber enables faster and more uniform freezing, dependent on load
Electrical	Ice nucleation induced by high voltage	Yes	++	---	---	---	++	Yes	x	Application in cryotubes, direct vs. Indirect electrofreezing

Table 1. Cont.

Freezing Method	Procedure	CN?	T _n	SSA	R _p	Primary Drying Time	Secondary Drying Time	Integration (Equipment Change Necessary?)	GMP	Comments
Ultrasound	Ice nucleation triggered with ultrasound wave	Yes	++	--	--	--	++	Yes	✓	High intra-vial heterogeneity, scale-up limited
Vacuum induced surface freezing	Vacuum inside chamber evaporates small amount of water on surface, self-cooling induces ice nucleation	Yes	++	--	-	-	++	No	✓	Easy scale-up, vacuum formulation dependent
Depressurization	Pressure shift from overpressure to atm shifts freezing point	Yes	++	--	-	--	++	No, only if equipment can withstand overpressure	✓	Efficiency connected with inert gas
Ice nucleating agents	Ice nucleating agent acts as nucleation site (e.g., AgI, P. syringae)	No	+	-	-	-	+	No	x	Great inter-vial heterogeneity, nucleation efficiency depends on concentration
Non-aqueous co-solvent	Ice crystal habit is changed by high-volatility co-solvent (e.g., TBA)	No	n.i.	--	-	--	++	No	x	Ice crystal size and morphology dependent on amount of co-solvent, organic solvents introduce safety risks
Vial modification	Vial pre-treatment such as scoring, scratching or roughening favors ice nucleation	No	-	+	+	+	-	No	x	Only marginal increase in nucleation temperature detectable

4. Materials and Methods

4.1. Product Mixture and Instruments

Saccharose solutions of 25 g/L were prepared with d(+)-saccharose (VWR Chemicals) and purified water (ariumTMpro, Sartorius AG, Göttingen, Germany). Weights were measured with a laboratory-scale LC 1200 S (Sartorius AG, Göttingen, Germany).

4.2. Experimental Runs

The freezing step was varied based on the Design of Experiments (DoE) as depicted in Table 2. The freezing method and dedicated process parameters were varied together with the fill volume. During shelf-ramped freezing without a holding step, the shelves were ramped at a dedicated ramp to $-45\text{ }^{\circ}\text{C}$. The hold time for shelf-ramped freezing with a holding step was 1 h. The final shelf temperature was $-45\text{ }^{\circ}\text{C}$ and the ramps were set to 1 K/min.

Table 2. Design of Experiments freezing step.

Freezing Method	Ramp (K/min)	Fill Volume (mL)
Shelf-ramped freezing without hold step	0.1	1
	2	1
	0.1	2
	2	2
	Hold temperature ($^{\circ}\text{C}$)	Fill volume (mL)
Shelf-ramped freezing with holding step	0	1
	-5	1
	0	2
	-5	2
	Shelf temperature ($^{\circ}\text{C}$)	Fill volume (mL)
Precooled	-30	1
	-45	1
	-30	2
	-45	2
	Nucleation temperature ($^{\circ}\text{C}$)	Fill volume (mL)
Ice fog method LyoCoN	-2	1
	-4	1
	-8	1
	-2	2
	-4	2
	-8	2

The ice fog experiments were performed with LyoCoN (Martin Christ Gefriertrocknungsanlagen GmbH, Osterode am Harz, Germany). During the LyoCoN experiments, the samples were equilibrated at the nucleation temperature for 30 min, then the chamber was evacuated to 4 mbar and subsequently aerated to introduce the ice crystals into the chamber.

The primary drying conditions are fixed for all experiments at $0\text{ }^{\circ}\text{C}$ and 0.15 mbar. The comparative pressure is used as the forwarding condition. The secondary drying was set to $40\text{ }^{\circ}\text{C}$ and 0.15 mbar. The final shelf temperature during secondary drying was achieved by a ramp of 0.5 K/min and held for 10 h.

4.3. Freeze-Drying Equipment

The freeze-drying experiments were carried out using a pilot-scale freeze-dryer shown in Figure 4 (Epsilon 2-6 LSCplus (Martin Christ Gefriertrocknungsanlagen GmbH, Osterode am Harz, Germany). A LyoCoN container was attached to the equipment to achieve controlled nucleation. LyoCoN is based on the ice fog technique. The container is attached

to the ice condenser chamber. During controlled nucleation, the freeze dryer is evacuated while the LyoCoN container remains under ambient pressure. As soon as the pressure value is reached, the LyoCoN container is connected to the ice condenser chamber, causing a pressure surge that carries away ice crystals that have been formed on the ice condenser into the drying chamber and the vials, leading to controlled nucleation without the necessity of external media. Only the moisture inside the freeze-dryer is used. 6R vials are used for the experiments and filled with 2 mL of product solution. The middle shelf is fully loaded with 135 vials. WTMplus sensors (Martin Christ Gefriertrocknungsanlagen GmbH, Osterode am Harz, Germany) measure the product temperature during primary drying. During the experiments, pictures of the vials are taken with the LyoCam (Martin Christ Gefriertrocknungsanlagen GmbH, Osterode am Harz, Germany) that is installed on the front door.



Figure 4. Epsilon 2-6D LSCplus with LyoCoN container (Copyright © Martin Christ Gefriertrocknungsanlagen GmbH).

4.4. Dry Layer Resistance

MTMplus (Martin Christ Gefriertrocknungsanlagen GmbH, Osterode am Harz, Germany) determines the dry layer resistance R_p . An optimized MTM is used every 10 min to ensure product safety while obtaining all necessary data. Here, the test is aborted as soon as no significant increase in chamber pressure is detected. The duration of the test varies depending on the pressure rise from 3 to 30 s.

4.5. Heat Flux Measurement

An FHF03 heat flux sensor (Hukesflux Thermal Sensors, Delft, The Netherlands) was used for heat flux measurement. The sensing area was 2.5 cm² and the temperature difference was measured by a thermopile. The sensor was placed on the front left side and fixed with adhesive tape (Scotch[®] adhesive tape 8915 (3M Deutschland GmbH, Neuss, Germany)).

4.6. Modeling

A pseudo-stationary model was used to calculate the dedicated primary drying end-point and product temperature of selected vials. The coupled heat and mass transfer can be written as [54]:

$$K_v \cdot (T_S - T_p) \cdot A_v = \frac{\Delta H_{\text{subl}}}{R_p} (p_i - p_c) \cdot A_p \quad (1)$$

R_p is the dry layer resistance, p_i is the partial vapor pressure on the sublimation interface, p_c is the chamber pressure and A_p the inner cross-sectional area of the vial. Table 3 shows the values of some parameters.

Table 3. Parameter for simulation.

Parameter	Value
A_v	3.8 cm ²
A_p	3.14 cm ²
ΔH_{subl}	2834.6 kJ/kg

This model has previously been validated for two different material systems [55,56].

4.7. Software

LPCplus (Martin Christ Gefriertrocknungsanlagen GmbH, Osterode am Harz, Germany) collected the data during freeze-drying runs, and the MTM data were analyzed with MTMplus Analyse (Martin Christ Gefriertrocknungsanlagen GmbH, Osterode am Harz, Germany). An LI-19 (Hukseflux Thermal Sensors, Delft, The Netherlands) collected the heat flux data. Aspen Custom Modeler (Aspen Technology, Inc., Bedford, MA, USA) was used for simulations.

5. Results

5.1. Nucleation Temperature

Several effects occur during freezing: cooling, supercooling, nucleation, and ice crystal growth. A further distinction is made between controlled and uncontrolled nucleation.

The product temperature profile of the shelf-ramped freezing without a holding step is shown in Figure 5a. The shelf temperature is continuously reduced, and the product is cooled over the temperature difference until nucleation occurs. The nucleation temperature is very broadly distributed, between -7 and -14 °C. With the LyoCam, pictures can be taken during the process. The cloudy vials have already started nucleation, while the clear vials are still undercooled (see Figure 5c). Figure 5b shows the product temperature profile for the shelf-temperature freezing with a holding step. Here, the shelf temperature is held at -5 °C for one hour to equilibrate the temperature across the sample. After this, the shelf is cooled down further and random nucleation between -8 and -12 °C occurs. Again, a picture of the LyoCam is shown, which shows the nucleation distribution well (see Figure 5d).

Next, the temperature profile of the pre-cooled shelf is shown in Figure 6a. The shelves are pre-cooled to the final temperature and only then are the samples loaded onto the shelves. There is a drastic decrease in the product temperature until nucleation occurs. It takes place in a range from -5 to -10 °C. The LyoCam also indicated the random distribution of the nucleation temperature (see Figure 6c).

Finally, the product temperature profile of an experiment with LyoCoN is shown. LyoCoN is an ice fog technique that can be used to control the nucleation time and temperature. Figure 6b shows the product temperature profile. The product is cooled down to the target temperature and the product is equilibrated. This step is important because the supercooling at the product surface must be high enough to nucleate using the ice mist. Once the product temperature is equilibrated, the chamber is evacuated, and a blast of pressure is used to move the ice crystals from the ice condenser into the drying chamber

onto the product surface. This has the major advantage that no external media are introduced into the freeze dryer. All vials nucleate at the same time, confirmed with the product temperature. Compared to all experiments before, the product temperature is clearly more homogeneous over the measured vials. The same point in time is also confirmed by the LyoCam (see Figure 6d).

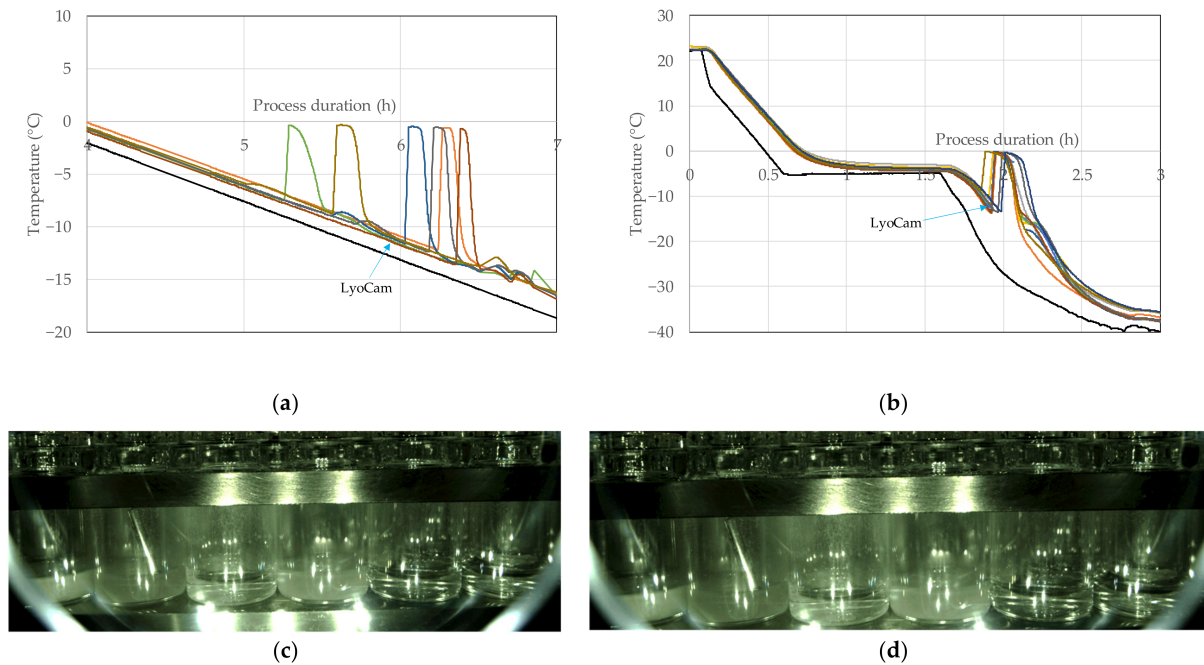


Figure 5. (a) Product temperature profile during shelf-ramped freezing (0.1 K/min, 1 mL) without hold step; (b) product temperature profile during shelf-ramped freezing with holding step ($-5\text{ }^{\circ}\text{C}$, 1 mL); (c) LyoCam picture shelf-ramped freezing (0.1 K/min, 1 mL); (d) LyoCam picture shelf-ramped freezing with holding step ($-5\text{ }^{\circ}\text{C}$, 1 mL).

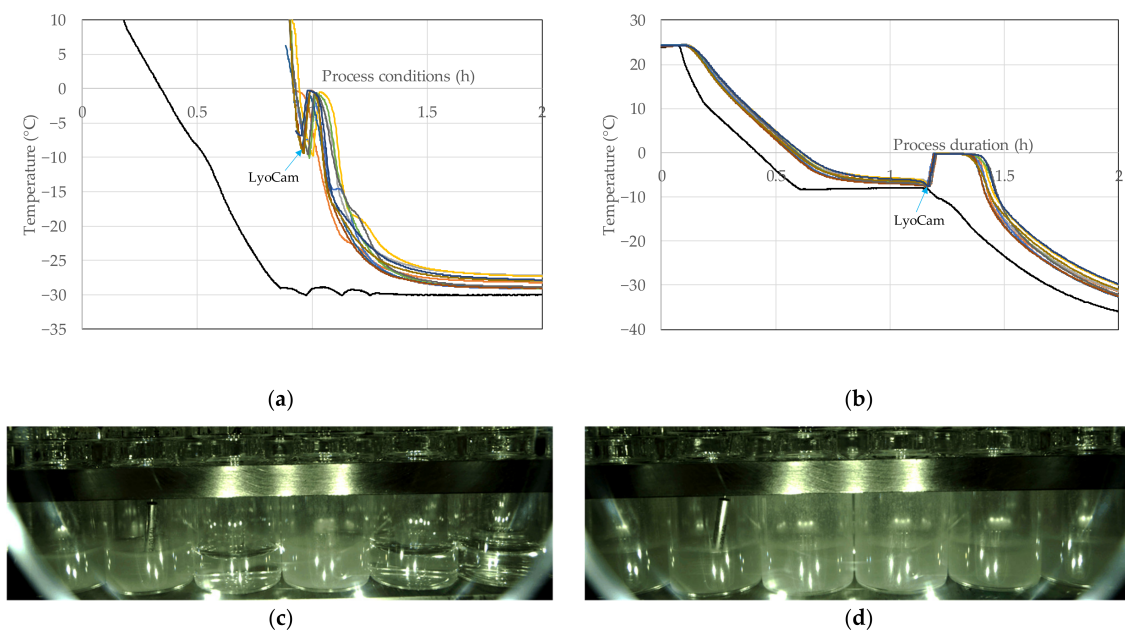


Figure 6. (a) Product temperature profile during pre-cooled shelf freezing ($-30\text{ }^{\circ}\text{C}$, 2 mL); (b) product temperature profile during LyoCoN freezing ($-8\text{ }^{\circ}\text{C}$, 2 mL); (c) LyoCam picture pre-cooled shelf freezing ($-30\text{ }^{\circ}\text{C}$, 2 mL); (d) LyoCam picture LyoCoN freezing ($-8\text{ }^{\circ}\text{C}$, 2 mL).

The nucleation temperature and its distribution are important process parameters, as they determine the ice crystal size and product morphology. Figure 7 shows the distributions.

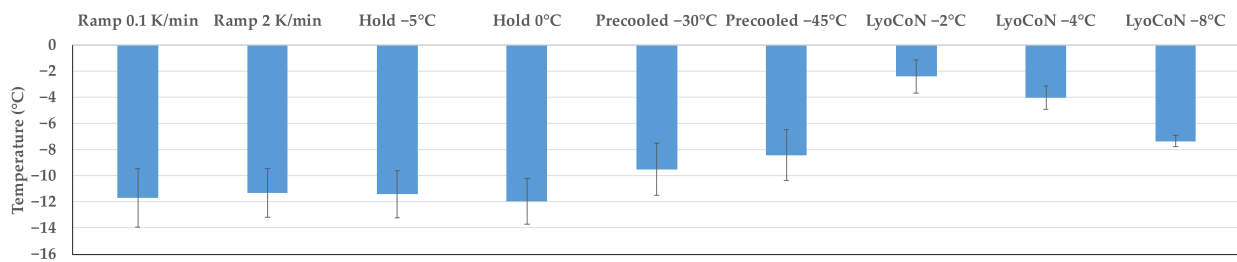


Figure 7. Nucleation temperature distribution for different freezing methods.

Shelf-cooled freezing with and without a holding step has a high supercooling of $-12\text{ °C} \pm 2\text{ °C}$. The pre-cooled shelf method has a lower supercooling of $-9\text{ °C} \pm 2\text{ °C}$, but the distribution here is also very broad as nucleation still occurs randomly. Only the experiments with LyoCoN can control the nucleation temperature. The nucleation temperatures are $-2.4\text{ °C} \pm 1.2\text{ °C}$ (LyoCoN -2 °C), $-4\text{ °C} \pm 0.9\text{ °C}$ (LyoCoN -4 °C) and $-7.4\text{ °C} \pm 0.4\text{ °C}$ (LyoCoN -8 °C). In all experiments, the nucleation temperature distribution is significantly lower than in the other experiments. As the shelf temperature decreases, the distribution also becomes smaller. This is due to the fact that in the three experiments, the chamber for the LyoCoN process was evacuated to 4 mbar. This pressure seems to be set too low for higher nucleation temperatures, which results in even small evaporation effects that cool the product further, resulting in a wider distribution. Thus, the process conditions of the shelf temperature and chamber pressure have to be carefully selected to obtain narrow nucleation temperature distributions with LyoCoN.

5.2. Heat Flux

The heat flux data for the individual tests for the ramped freezing are shown in Figure 8a for a ramp of 0.1 K/min. The product is cooled down to nucleation at a constant cooling rate. At 0.1 K/min, the heat flux in the cooling step was approximately -100 W/m^2 for 1 mL and -150 W/m^2 for 2 mL, respectively. Increasing the cooling rate to 2 K/min increases the heat flux to -570 W/m^2 for 1 mL or 745 W/m^2 for 2 mL. The increased cooling rate causes the temperature difference between the shelf and the product to increase, resulting in increased heat flux.

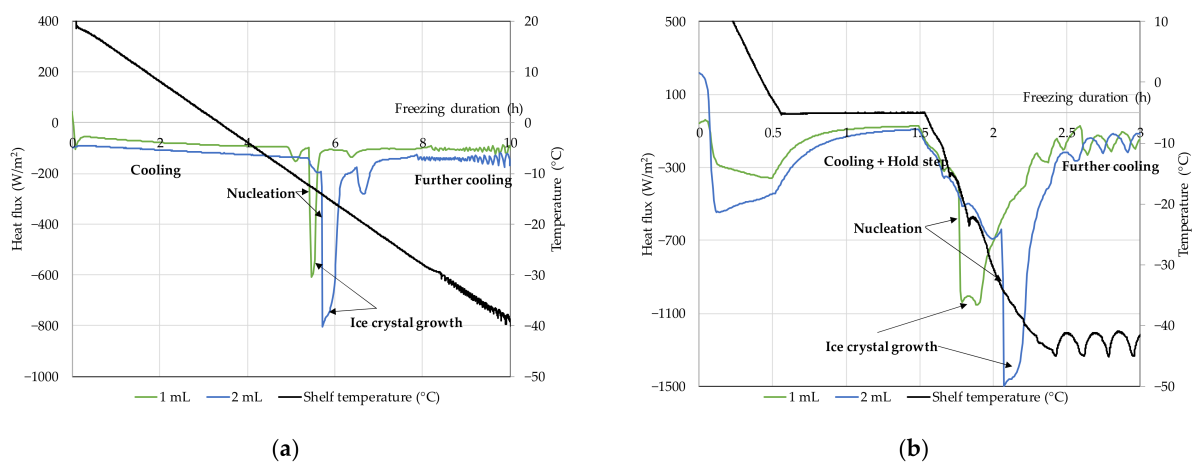


Figure 8. Heatflux data: (a) shelf-ramped freezing (0.1 K/min); (b) shelf-ramped freezing with holding step at -5 °C .

After the product has been sufficiently supercooled, nucleation occurs. In the product temperature profile, this can be seen by a sharp rise to 0 °C, and heat flow signal nucleation can also be seen by a sharp fall. Nucleation is an exothermic process that releases heat. Nucleation takes place at different times. At a cooling rate of 0.1 K/min, nucleation takes place at 5.4 h for a filling volume of 1 mL and at 5.6 h for 2 mL. The heat flux decreases to minimum values of -607 W/m^2 (1 mL) and -804 W/m^2 (2 mL). A cooling rate of 2 K/min shifts the nucleation time forward to 0.63 h (1 mL) and 0.83 h (2 mL). The minimum heat flux decreases to -1493 W/m^2 at 1 mL and -1502 W/m^2 at 2 mL.

After nucleation, there is further ice crystal growth and final cooling to the steady-state shelf temperature.

Figure 8b shows the heat flux data of the shelf-ramped freezing with a holding step at -5 °C . Here, too, the product is cooled continuously until the holding step. At a holding step of -5 °C , the heat flux is a minimum of -320 W/m^2 (1 mL) or -510 W/m^2 (2 mL). Subsequently, the heat flux approaches 0 W/m^2 , which induces that the holding step is sufficiently long. Nucleation releases a heat flux of -1256 W/m^2 (1 mL, 0 °C), -1549 W/m^2 (2 mL, 0 °C), -1040 W/m^2 (1 mL, -5 °C) and -1483 W/m^2 (2 mL, -5 °C), respectively. Here, too, nucleation takes place at different times.

Figure 9a shows the heat flow data for the tests with the pre-cooled shelf. As soon as the product is loaded into the freeze dryer, there is a drastic drop in heat flux due to the high temperature difference. The product is cooled with an initial heat flux of -2695 W/m^2 (1 mL, -30 °C), -2511 W/m^2 (2 mL, -30 °C), -2691 W/m^2 (1 mL, -45 °C) or -2663 W/m^2 (2 mL, -45 °C). As time progresses, the product temperature approaches the shelf, causing the heat flux to decrease. Subsequently, nucleation occurs. Since the shelf has already reached its stationary end value, the temperature difference after nucleation remains constant for the time being. This is a post-nucleation hold.

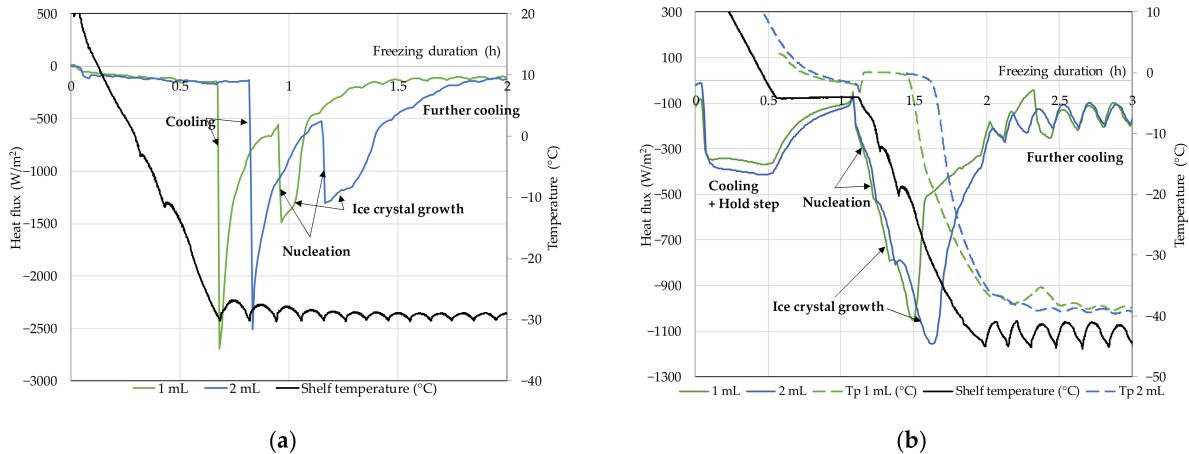


Figure 9. Heatflux data: (a) pre-cooled shelf at -30 °C ; (b) LyoCoN freezing at -4 °C .

Figure 9b shows the heat flow data for LyoCoN experiments at -4 °C . First, the product is cooled down. A heat flux of -329 W/m^2 (1 mL, -2 °C), -440 W/m^2 (2 mL, -2 °C), -367 W/m^2 (1 mL, -4 °C) and -409 W/m^2 (2 mL, -4 °C) is transferred. Due to the holding step, the heat flux approaches 0 W/m^2 . As soon as nucleation has been induced, the heat flux increases significantly because the surface is cooled down again, which leads to an increase in the temperature difference. The minimum heat flux is -842 W/m^2 (1 mL, -2 °C), -1217 W/m^2 (2 mL, -2 °C), -1044 W/m^2 (1 mL, -4 °C) and -1153 W/m^2 (2 mL, -4 °C). With the help of LyoCoN, the nucleation temperature of the vials can be controlled. This leads to a more reproducible and also comparable freezing behavior in relation to the other freezing steps.

Ice fog is the only freezing method that controls the nucleation temperature, meaning that not only is the nucleation temperature controlled throughout the batch but the freezing

behavior between different fill volumes is aligned and shows similar behaviors and heat fluxes. A summary of the heat flux results is depicted in Table 4.

Table 4. Heat flux data for different freezing methods.

Freezing Method	Ramp (K/min)	Heat Flux Cooling (W/m ²)		Heat Flux Nucleation (W/m ²)	
		1 mL	2 mL	1 mL	2 mL
Shelf-ramped freezing without hold step	0.1	−100	−150	−607	−804
	2	−500	−745	−1493	−1502
	Hold temperature (°C)				
Shelf-ramped freezing with holding step	0	−265	−410	−1256	−1549
	−5	−320	−510	−1040	−1483
	Shelf temperature (°C)				
Precooled	−30	−2695	−2511	−1490	−1294
	−45	−2691	−2663	−1656	−1780
	Nucleation temperature (°C)				
Ice fog method LyoCoN	−2	−329	−440	−842	−1217
	−4	−367	−409	−1044	−1153
	−8	−350	−420	−1136	−1263

5.3. Dry Layer Resistance

MTM can be used to determine the dry layer resistance during primary drying. It depends on the ice crystal size and distribution. A high resistance leads to slow drying kinetics and higher product temperatures. For optimal primary drying, a reproducible, low dry layer resistance that is constant across all vials is ideal.

Figure 10a shows the dry layer resistance for freezing with ramped shelves without a holding step. In general, freezing at 0.1 K/min shows a significantly higher dry layer resistance than freezing at 2 K/min, although the nucleation temperatures are equally distributed here. The dry layer resistance for cooling at 0.1 K/min starts at 39,174 m/s ± 7424 m/s and increases linearly to a final value of 248,952 m/s ± 180,984 m/s. At a cooling rate of 2 K/min, the dry layer resistance starts at 49,805 m/s ± 38,025 m/s, increases to 79,750 m/s ± 40,495 m/s (dry film height 0.001 m) and ends at 87,732 m/s ± 33,526 m/s.

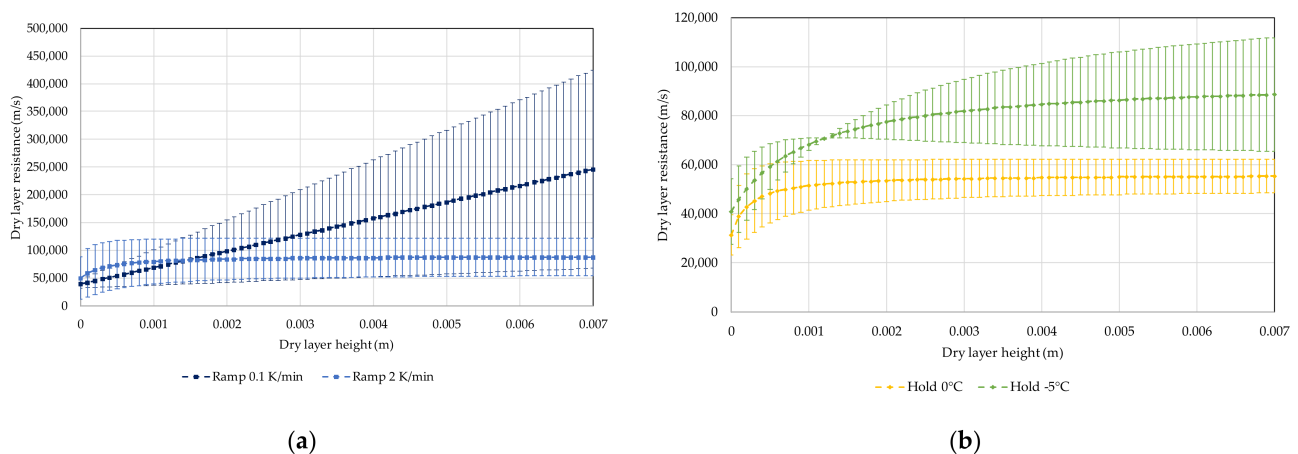


Figure 10. Dry layer resistance. (a) Shelf-ramped freezing with various ramps; (b) shelf-ramped freezing with holding step at different temperatures.

A slow cooling rate significantly prolongs the process and results in significantly higher and highly fluctuating dry layer resistances.

Figure 10b shows the dry film resistances for freezing with ramped shelves with a holding step.

With a holding step of $-5\text{ }^{\circ}\text{C}$, the dry layer resistance starts at $40,899\text{ m/s} \pm 13,360\text{ m/s}$ and increases asymptotically to a final value of $88,669\text{ m/s} \pm 23,175\text{ m/s}$. If the holding step is applied at $0\text{ }^{\circ}\text{C}$, the dry film resistance has an initial value of $31,378\text{ m/s} \pm 8179\text{ m/s}$ and also increases asymptotically to $55,304\text{ m/s} \pm 6815\text{ m/s}$. The resistance shows lower values and deviations when applying an equilibration step compared to shelf-ramped cooling.

Figure 11a shows the dry layer resistances for freezing with pre-cooled shelves. Both shelf temperatures show an asymptotic curve. The dry layer resistance starts at $15,494\text{ m/s} \pm 15,469\text{ m/s}$ ($-30\text{ }^{\circ}\text{C}$) and $16,719\text{ m/s} \pm 115\text{ m/s}$ ($-45\text{ }^{\circ}\text{C}$) and then increases rapidly to the final value ($72,881\text{ m/s} \pm 15,836\text{ m/s}$ at $-30\text{ }^{\circ}\text{C}$ and $52,018\text{ m/s} \pm 2295\text{ m/s}$ at $-45\text{ }^{\circ}\text{C}$). The use of pre-cooled shelves increases the nucleation temperature, resulting in less supercooling, which leads to the formation of larger ice crystals, thus reducing the resistance of the dry layer.

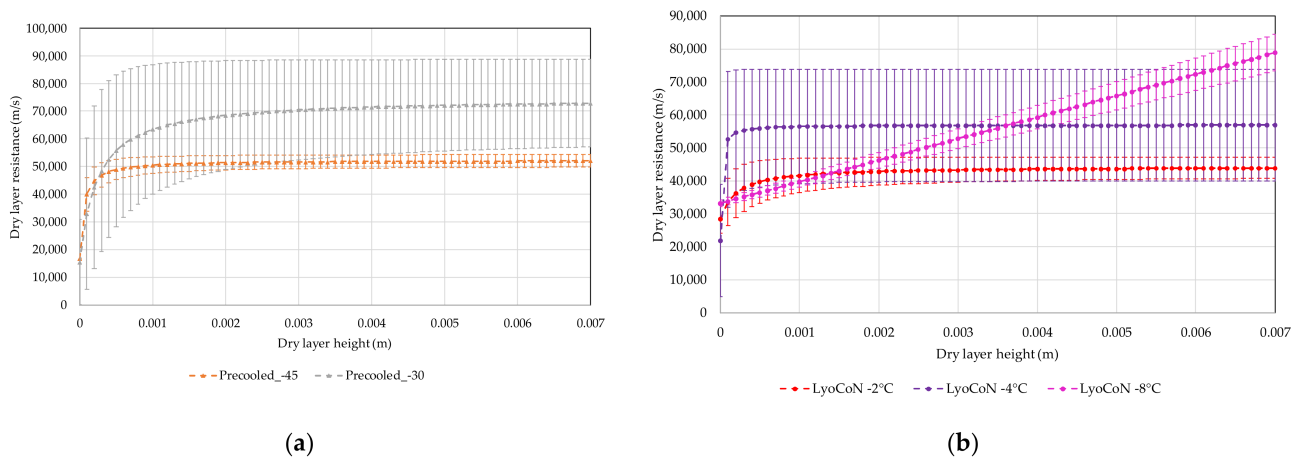


Figure 11. Dry layer resistance. (a) Precooled shelves at different temperatures; (b) ice fog at various nucleation temperatures.

In Figure 11b, the dry layer resistance for freezing with ice fog at different nucleation temperatures is shown. Experiments with nucleation temperatures of -2 and $-4\text{ }^{\circ}\text{C}$ show asymptotic behavior, while at $-8\text{ }^{\circ}\text{C}$, a linear course can be observed. The dry layer resistances begin at $28,353\text{ m/s} \pm 4273\text{ m/s}$ ($-2\text{ }^{\circ}\text{C}$), $21,851\text{ m/s} \pm 16,929\text{ m/s}$ ($-4\text{ }^{\circ}\text{C}$) and $33,161\text{ m/s} \pm 1047\text{ m/s}$ ($-8\text{ }^{\circ}\text{C}$) and increase to $43,853\text{ m/s} \pm 3168\text{ m/s}$ ($-2\text{ }^{\circ}\text{C}$), $56,838\text{ m/s} \pm 16,912\text{ m/s}$ ($-4\text{ }^{\circ}\text{C}$) and $79,471\text{ m/s} \pm 5610\text{ m/s}$ ($-8\text{ }^{\circ}\text{C}$). The asymptotic course for -2 and $-4\text{ }^{\circ}\text{C}$ could indicate that the pressure value has been set too low, causing slight evaporation on the surface. This leads to increased supercooling; therefore, this small layer has the highest resistance to vapor flow.

Shelf-ramped freezing with no holding step shows the highest dry layer resistance along with the highest uncertainty. Random nucleation at a high supercooling and non-equilibrated solution provides high variance. If a hold step is added, the temperature is equalized over the product, reducing the variance and mean values of R_p . If the nucleation temperature is lowered, the variance and mean value can be further reduced. With the appropriate freezing step, the dry layer resistance can be more than halved from $87,732\text{ m/s}$ to $43,853\text{ m/s}$, and the variance is reduced from $33,526\text{ m/s}$ to 3168 m/s by 90%. A summary of the dry layer resistances is shown in Table 5.

Table 5. Dry layer resistances of different freezing methods.

Freezing Method	Ramp (K/min)	Dry Layer Resistance (m/s)		
		$L_{\text{dry}} = 0 \text{ m}$	$L_{\text{dry}} = 0.0035 \text{ m}$	$L_{\text{dry}} = 0.007 \text{ m}$
Shelf-ramped freezing without hold step	0.1	$39,174 \pm 7424$	$142,585 \pm 92,982$	$248,952 \pm 180,984$
	2	$49,805 \pm 38,025$	$86,119 \pm 35,193$	$87,732 \pm 33,526$
Hold temperature ($^{\circ}\text{C}$)				
Shelf-ramped freezing with holding step	0	$31,378 \pm 8179$	$54,557 \pm 7559$	$55,304 \pm 6815$
	-5	$40,899 \pm 13,360$	$83,425 \pm 15,071$	$88,669 \pm 23,175$
Shelf temperature ($^{\circ}\text{C}$)				
Precooled	-30	$15,494 \pm 15,469$	$71,046 \pm 17,543$	$72,881 \pm 15,836$
	-45	$16,719 \pm 115$	$51,754 \pm 2428$	$52,018 \pm 2295$
Nucleation temperature ($^{\circ}\text{C}$)				
Ice fog method LyoCoN	-2	$28,353 \pm 4273$	$43,422 \pm 3607$	$43,853 \pm 3168$
	-4	$21,851 \pm 16,929$	$56,767 \pm 16,984$	$56,838 \pm 16,912$
	-8	$33,161 \pm 1047$	$55,990 \pm 3296$	$79,471 \pm 5610$

5.4. Primary Drying Endpoint

Next, the experimental primary drying endpoint is compared to simulation results. The freezing step controls the dry layer resistance and therefore the drying kinetics of each individual vial.

Figure 12 shows the experimental and simulated primary drying endpoint for an edge at different freezing steps in a parity plot. The x-axis shows the experimental and the y-axis the simulated primary drying endpoint. The largest deviation between simulation and experiment is achieved with the freezing method Ramp 0.1 K/min. Here, an endpoint of $4.6 \text{ h} \pm 0.5 \text{ h}$ is calculated and experimentally determined at $2.3 \text{ h} \pm 0.2 \text{ h}$. The very high dry layer resistance combined with a very high uncertainty ensures that the simulation overestimates the primary drying endpoint. The situation is different with the LyoCoN experiments. They generate very narrowly distributed and low dry layer resistances. For LyoCoN $-2 \text{ }^{\circ}\text{C}$, a primary drying endpoint is determined at $3.4 \text{ h} \pm 0.05 \text{ h}$; for LyoCoN, $-4 \text{ }^{\circ}\text{C}$ at $3.4 \text{ h} \pm 0.05$; and for LyoCoN, $-8 \text{ }^{\circ}\text{C}$ at $3.3 \text{ h} \pm 0.07 \text{ h}$. Experimentally, the endpoints here are very close to each other. Experimentally, the endpoints here are $3.05 \text{ h} \pm 0.05 \text{ h}$ (LyoCoN $-2 \text{ }^{\circ}\text{C}$ and $-4 \text{ }^{\circ}\text{C}$) and $2.9 \text{ h} \pm 0.1 \text{ h}$. Due to the controlled nucleation, the simulation was able to describe the experiment much more accurately.

Similar results can be seen with a fill volume of 2 mL. The experiment without controlled nucleation shows high deviation between experiments and simulations. Ramp 0.1 K/min calculates the primary drying endpoint at $7 \text{ h} \pm 0.4 \text{ h}$ (experiment: $5.35 \text{ h} \pm 0.15 \text{ h}$), Ramp 2 K/min at $6.6 \text{ h} \pm 0.5 \text{ h}$ (experiment: $5.65 \text{ h} \pm 0.65 \text{ h}$), Hold $0 \text{ }^{\circ}\text{C}$ at $6.2 \text{ h} \pm 0.4 \text{ h}$ (experiment: $5.4 \text{ h} \pm 1 \text{ h}$) and Hold $-5 \text{ }^{\circ}\text{C}$ at $6.6 \text{ h} \pm 0.35 \text{ h}$ (experiment: $4.9 \text{ h} \pm 0.7 \text{ h}$). The best results are achieved with LyoCoN at $-2 \text{ }^{\circ}\text{C}$ and precooled shelves of $-45 \text{ }^{\circ}\text{C}$. The calculated endpoints are $6.1 \text{ h} \pm 0.5 \text{ h}$, respectively, $6.1 \text{ h} \pm 0.3 \text{ h}$, while the experiments are finished at $5.8 \text{ h} \pm 0.3 \text{ h}$ or $6.2 \text{ h} \pm 0.55 \text{ h}$.

The same observations can be seen in the center vial (see Figure 13). At a 1 mL fill volume, shelf-ramped freezing without hold steps shows the highest deviation (simulation: $6 \text{ h} \pm 0.7 \text{ h}$, experiment: $3.25 \text{ h} \pm 0.7 \text{ h}$). The experiments with LyoCoN and precooled shelves show the best agreement.

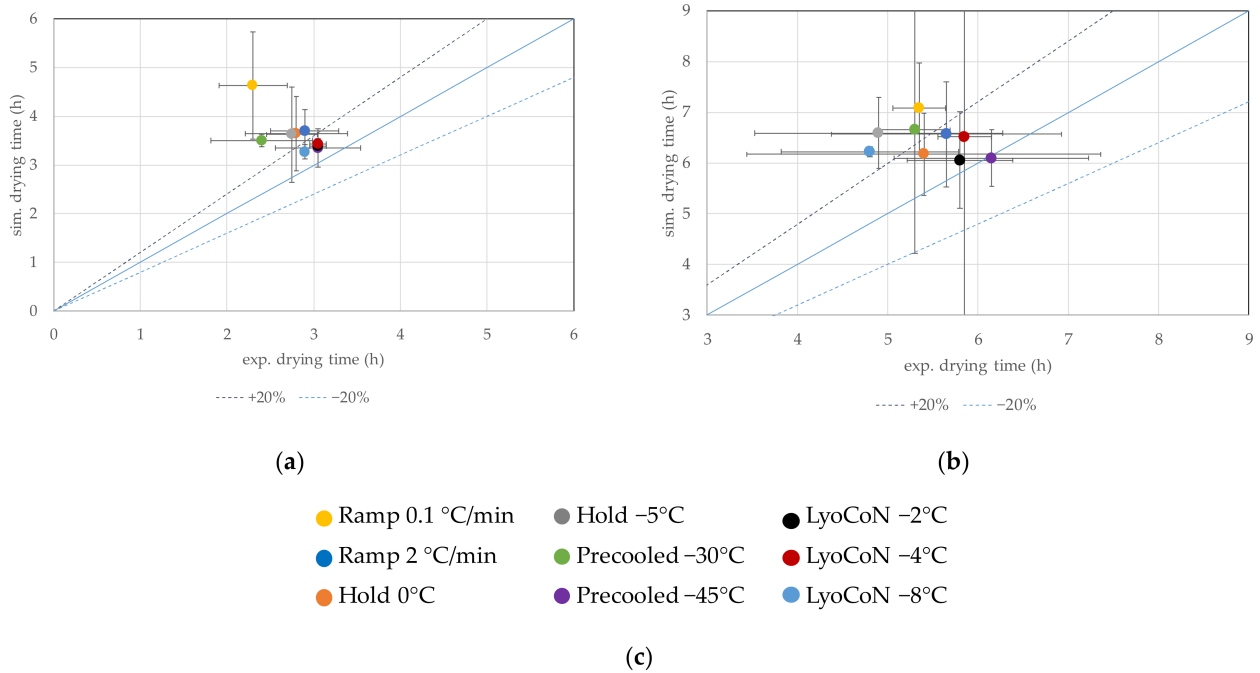


Figure 12. Primary drying endpoint for an edge vial: (a) 1 mL, (b) 2 mL, (c) legend.

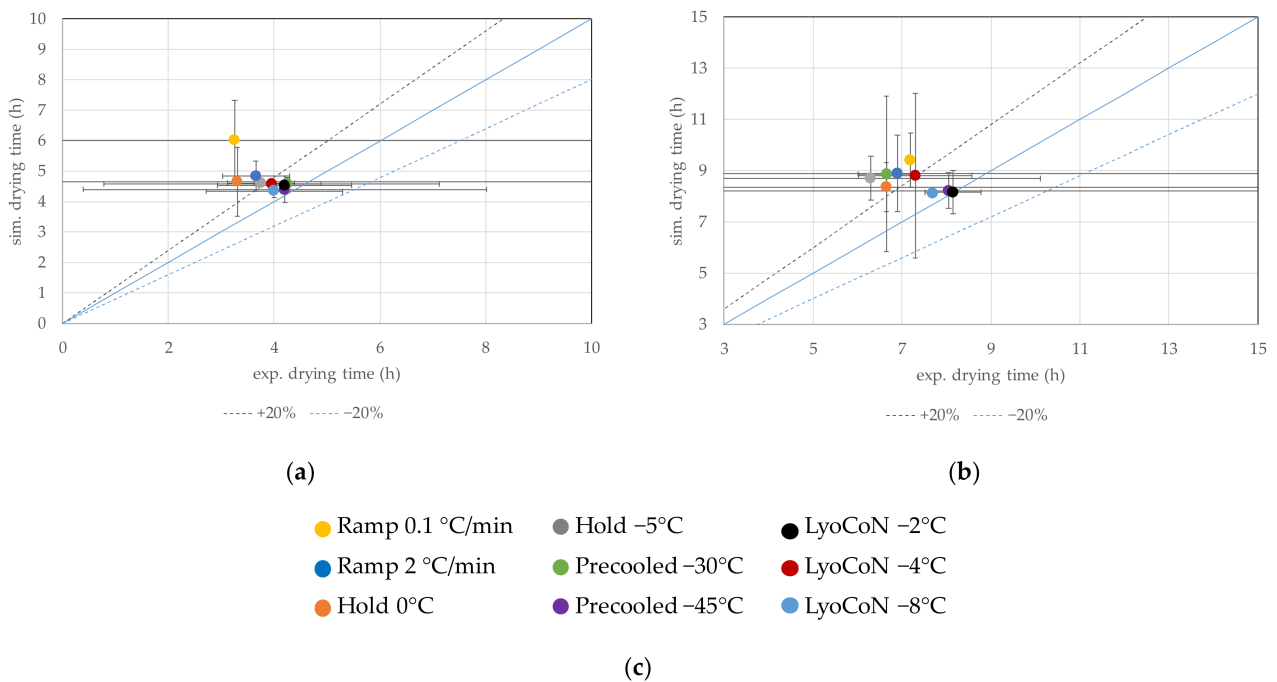


Figure 13. Primary drying endpoint for a center vial: (a) 1 mL, (b) 2 mL, (c) legend.

With increased fill volume, LyoCoN $-2\text{ }^{\circ}\text{C}$ and precooled $-45\text{ }^{\circ}\text{C}$ show the best agreement for the center vial. Controlled nucleation homogenizes the freezing of center vials, resulting in a more representative dry layer resistance measured by MTM.

Generally, the center vials take longer to dry than the edge vials, causing batch heterogeneity in the drying duration. It is shown in Figure 14 for different fill volumes as an absolute value. For 1 mL, the absolute batch heterogeneity is smaller. Controlled nucleation can further reduce heterogeneity. For 1 mL, the heterogeneities with LyoCoN are 1.85 h ($-2\text{ }^{\circ}\text{C}$), 2 h ($-4\text{ }^{\circ}\text{C}$) and 1.95 h ($-8\text{ }^{\circ}\text{C}$), while it increases with shelf-ramped freezing to 2.8 (0.1 K/min), respectively, 2.6 h (2 K/min). Simulation and experiment show good

agreement. For 2 mL, the heterogeneities with LyoCoN are 4.55 h ($-2\text{ }^{\circ}\text{C}$), 3.3 h ($-4\text{ }^{\circ}\text{C}$) and 4.05 h ($-8\text{ }^{\circ}\text{C}$), while it increases with shelf-ramped freezing to 4.55 (0.1 K/min), respectively, 4.8 h (2 K/min). The simulations again show good agreement with the experiments and can quantify the batch heterogeneity.

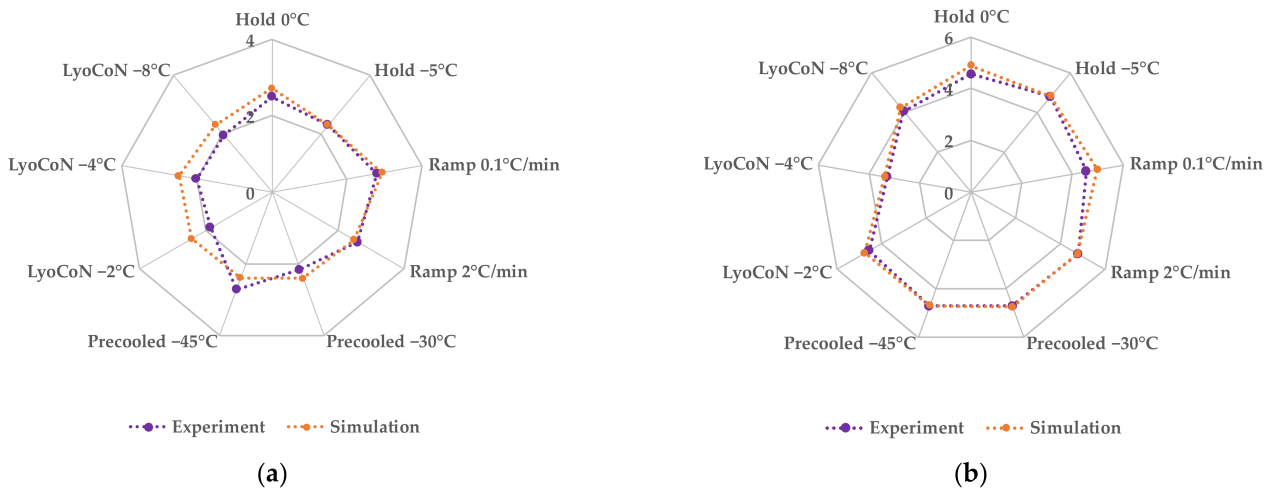


Figure 14. Batch heterogeneity: (a) 1 mL; (b) 2 mL.

5.5. Product Temperature

Besides the primary drying endpoint, the product temperature is another important parameter that can be predicted by the model. In this section, the different product temperatures that occur due to the different freezing methods in primary drying are presented for edge and center vials. In the figures, the primary drying endpoint is marked by a vertical line with its uncertainty.

Figure 15 shows the product temperatures of primary drying for freezing with a ramp of $0.1\text{ K}/\text{min}$ and 1 mL filling volume. A clear discrepancy between the experiment and simulation can be seen, both for the edge and the center vial. For the edge vial, a product temperature of $-21.9 \pm 1.8\text{ }^{\circ}\text{C}$ is averaged, but the experimental product temperature in primary drying reaches only $-32 \pm 2\text{ }^{\circ}\text{C}$. The center vial reaches a lower average product temperature of $-24.5 \pm 2\text{ }^{\circ}\text{C}$ in the simulation than the edge vial. However, this value is again higher than the experimentally determined one of $-34\text{ }^{\circ}\text{C} \pm 2\text{ }^{\circ}\text{C}$. The high uncertainty at the end of the experimental product temperature is due to the fact that the primary drying time varies greatly in these tests causing large differences.

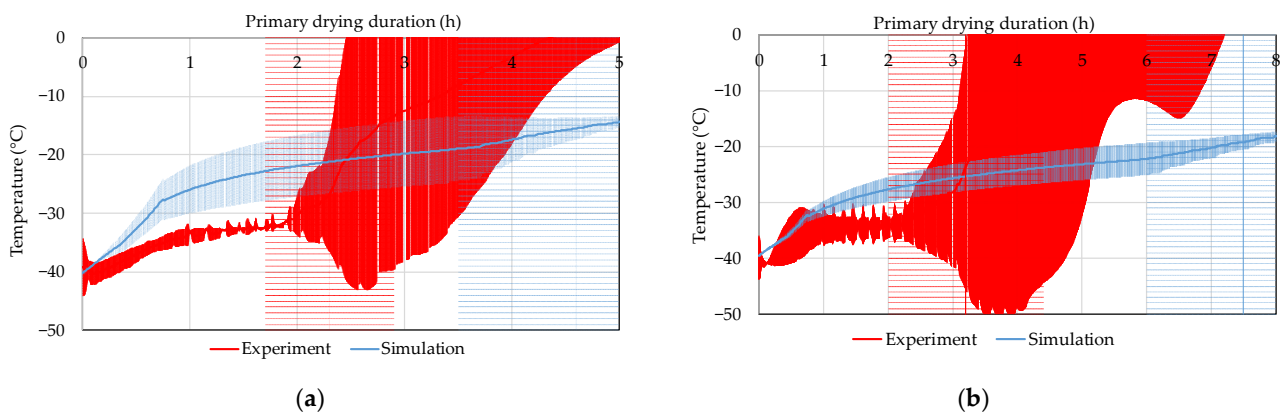


Figure 15. Experimental (red) and simulated (blue) primary drying product temperature with shelf-ramped freezing $0.1\text{ K}/\text{min}$ and 1 mL fill volume: (a) edge vial; (b) center vial.

Figure 16 shows the product temperature profile for an edge and middle vial at a freezing step of Ramp 2 K/min and a filling volume of 2 mL. For the edge vial, an average product temperature of -27.1 ± 1.9 °C is calculated, while an experimental value of -32.6 ± 2 °C is obtained. The difference between the simulation and the experiment could be reduced here. The middle vial has an average product temperature of -30.4 ± 1.9 °C in the simulation and -33.8 ± 1.5 °C in the experiment. Here, the simulation and experiment converge even further. The intersection of the simulated and experimental product temperature is at the primary drying endpoint.

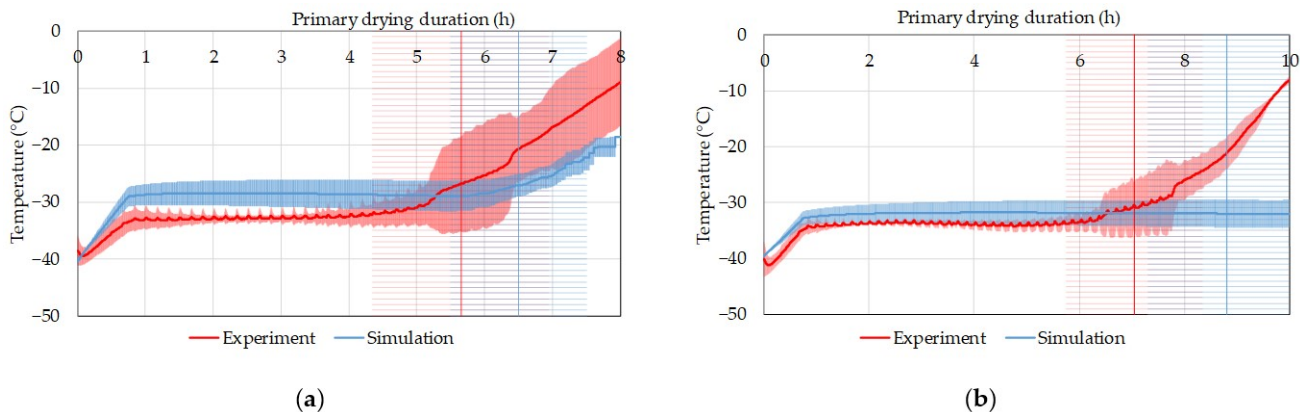


Figure 16. Experimental (red) and simulated (blue) primary drying product temperature with shelf-ramped freezing 2 K/min and 2 mL fill volume: (a) edge vial; (b) center vial.

Figure 17 shows the product temperature profiles for freezing with a holding step at -5 °C and a fill volume of 1 mL. Here, the product temperature profiles of the simulation and the experiments match well. In the corner vial, a simulated product temperature of -31.6 ± 0.5 °C is reached on average. At the beginning, the product temperatures overlap very well and then the simulation overestimates the product temperature by 0.6 °C. As soon as the primary drying comes to an end, the product temperatures overlap again. The center vial shows good agreement with the experiments over the entire primary drying period. Only a slight overestimation can be seen. An average product temperature of -33.5 ± 0.3 °C is reached in the simulation.

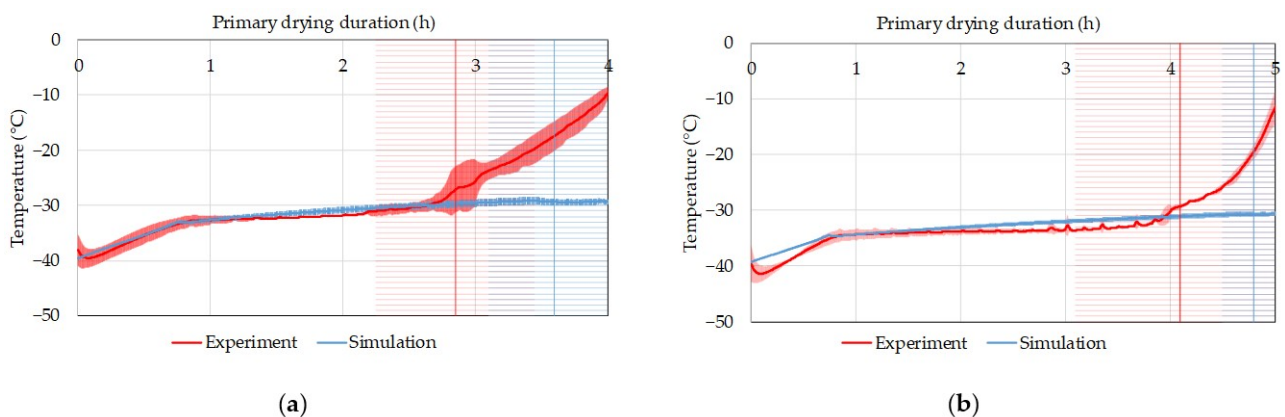


Figure 17. Experimental (red) and simulated (blue) primary drying product temperature with shelf-ramped freezing with hold step at -5 °C and 1 mL fill volume: (a) edge vial; (b) center vial.

Next, the product temperatures for freezing with a hold step at 0 °C are shown. They are shown in Figure 18. Again, the simulation overestimates the product temperature of the experiments in the edge vials. An average temperature of -30 ± 2.5 °C is calculated, while experimentally it is -33 ± 1 °C. As soon as the primary drying of the experiments comes

to an end, the results match well again. The product temperatures of the center vials match well. In the simulation, an average product temperature of $-33.3 \pm 2^\circ\text{C}$ is obtained. The experimental product temperature fits very well into the spanned band of the simulation with $-34 \pm 1^\circ\text{C}$ throughout the primary drying phase.

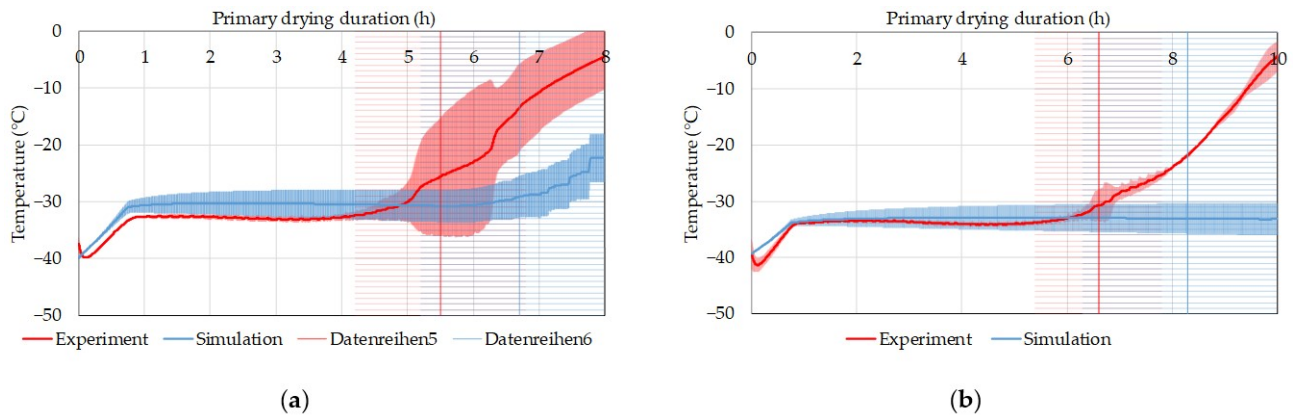


Figure 18. Experimental (red) and simulated (blue) primary drying product temperature with shelf-ramped freezing with hold step at 0°C and 2 mL fill volume: (a) edge vial; (b) center vial.

The product temperatures of the pre-cooled shelf at -30°C show similar results for a filling volume of 1 mL (see Figure 19). The product temperature of the corner vial is slightly overestimated in the simulation with $-30.9 \pm 0.7^\circ\text{C}$ (experiment: $-32 \pm 1^\circ\text{C}$). The product temperatures of the middle vial match better (simulation: $-32.8 \pm 0.5^\circ\text{C}$, experiment: $-32.6 \pm 1^\circ\text{C}$).

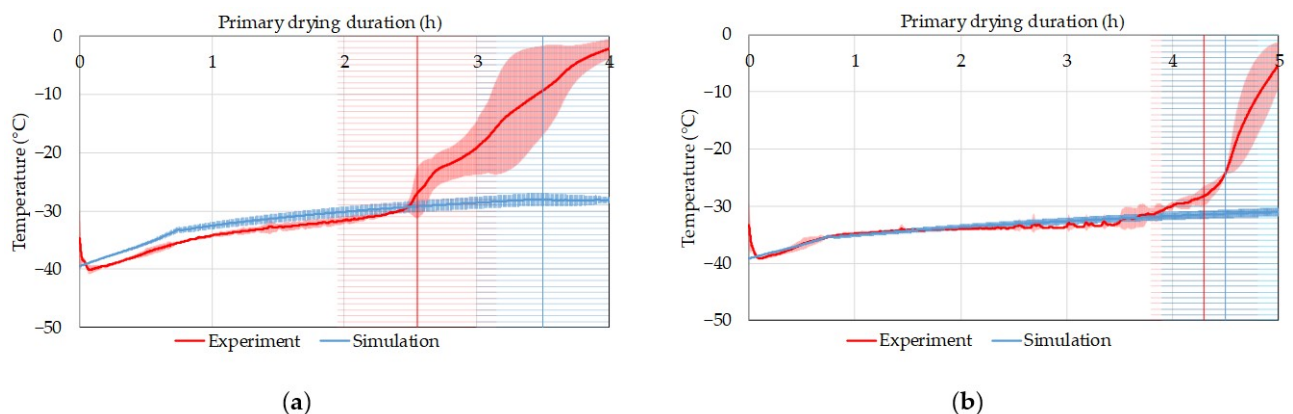


Figure 19. Experimental (red) and simulated (blue) primary drying product temperature with pre-cooled shelves at -30°C and 1 mL fill volume: (a) edge vial; (b) center vial.

The experimental and calculated product temperatures for a filling volume of 2 mL with the freezing method pre-cooled shelves -45°C are shown in Figure 20. The calculated and experimental results fit well together. In the corner vial, the product temperature is slightly overestimated at the beginning, and towards the end, the average values converge. In the simulation, an average product temperature of $-31.3 \pm 1.4^\circ\text{C}$ is obtained. In the experiment, the temperature is $-32.6 \pm 1.5^\circ\text{C}$.

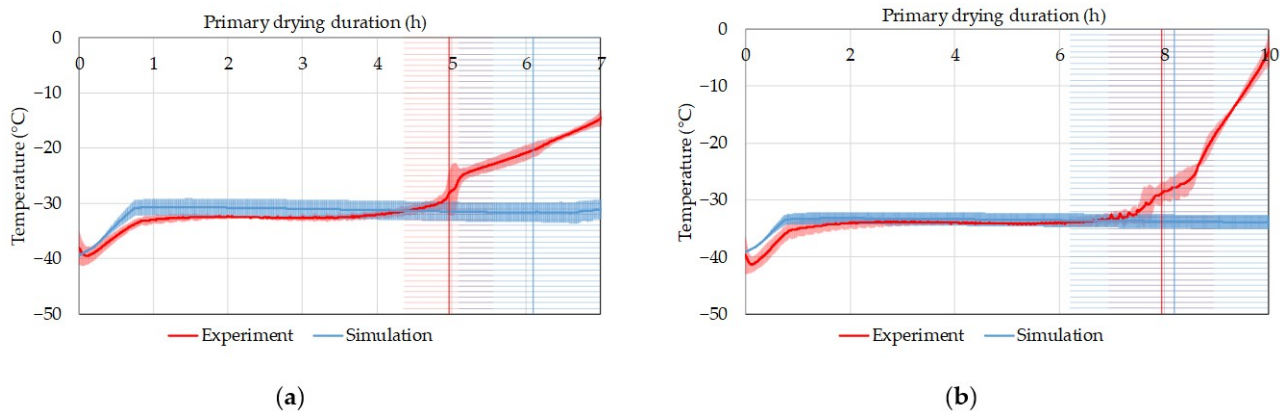


Figure 20. Experimental (red) and simulated (blue) primary drying product temperature with pre-cooled shelves at $-45\text{ }^{\circ}\text{C}$ and 2 mL fill volume: (a) edge vial; (b) center vial.

Finally, the product temperature profiles generated using LyoCoN are shown. None of the previous freezing methods controlled the nucleation, so it occurred randomly over a very wide range, resulting in each vial having its own temperature history and thus its own dry layer resistance. Figure 21 shows the product temperature history of the simulation and the experiments at a nucleation temperature of $-8\text{ }^{\circ}\text{C}$ and 1 mL filling volume. For both the edge and middle vials, the results show outstanding agreement. In the edge vial, the average calculated temperature is $-32.2 \pm 0.7\text{ }^{\circ}\text{C}$ (experiment: $-32.1 \pm 2\text{ }^{\circ}\text{C}$), and in the middle vial, it is $-34.1 \pm 0.5\text{ }^{\circ}\text{C}$ (experiment: $-33.9 \pm 2\text{ }^{\circ}\text{C}$). Both the absolute values and the curves of the product temperatures fit together well.

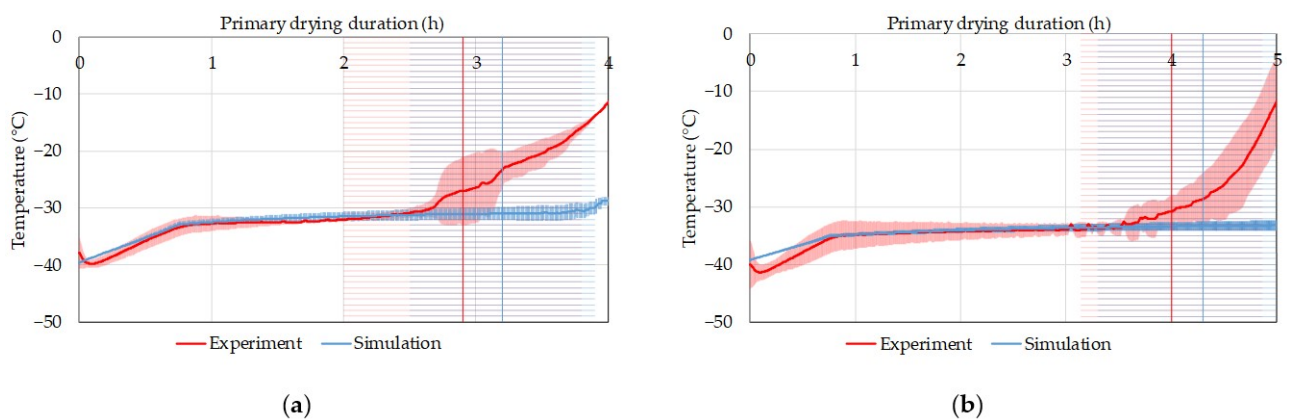


Figure 21. Experimental (red) and simulated (blue) primary drying product temperature with LyoCoN at $-8\text{ }^{\circ}\text{C}$ and 1 mL fill volume: (a) edge vial; (b) center vial.

Figure 22 shows the product temperatures for a controlled nucleation at $-4\text{ }^{\circ}\text{C}$ and a filling volume of 2 mL. The product temperature of the corner vial is slightly overestimated at the beginning and is in the simulation band from the middle of primary drying. The average product temperature was calculated as $-30.6 \pm 3.6\text{ }^{\circ}\text{C}$ and determined to be $-33.6 \pm 2\text{ }^{\circ}\text{C}$ in the experiments. The product temperature of the middle vials is slightly overestimated at the beginning and correctly predicted after a quarter of the primary drying. The calculated average product temperature is $-31.7 \pm 3.7\text{ }^{\circ}\text{C}$ and the experimental one is $-34 \pm 0.9\text{ }^{\circ}\text{C}$.

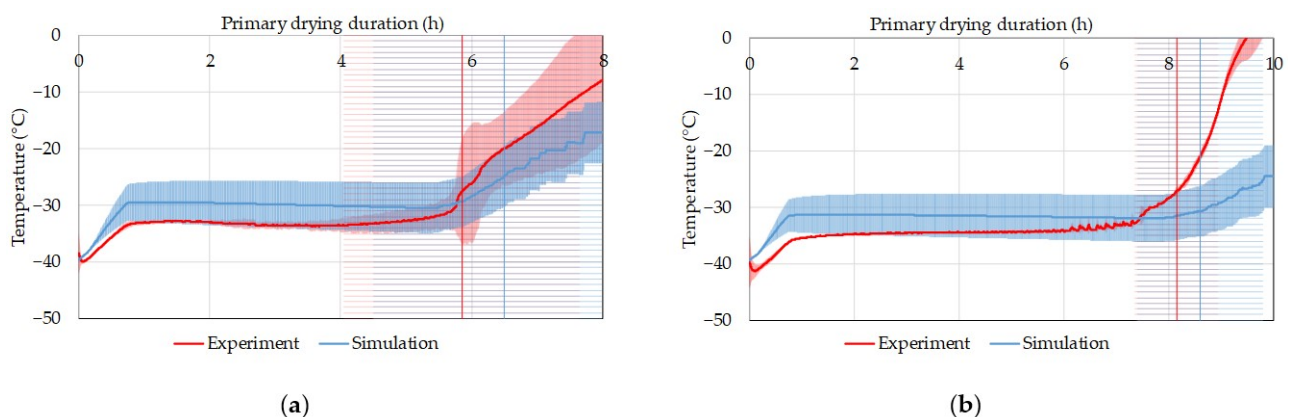


Figure 22. Experimental (red) and simulated (blue) primary drying product temperature with LyoCoN at $-4\text{ }^{\circ}\text{C}$ and 2 mL fill volume: (a) edge vial; (b) center vial.

6. Discussion

In this work, the influence of the freezing step on primary drying experiments and simulations were evaluated. The nucleation temperature cannot be controlled for the freezing methods of surface-controlled freezing with and without a holding step and precooled surfaces. Its range is $-11 \pm 3\text{ }^{\circ}\text{C}$, with pre-cooled shelves having a slightly higher nucleation temperature of $-9 \pm 3\text{ }^{\circ}\text{C}$. Experiments with LyoCoN can control the nucleation temperature and reduce the distribution (T_n ($-8\text{ }^{\circ}\text{C}$): $-7.5 \pm 0.5\text{ }^{\circ}\text{C}$). The freezing steps were tested for two filling volumes of 1 and 2 mL. The heat flux data for all experiments were determined. Throughout the freezing experiments with random nucleation, the data deviate. Only controlled nucleation obtains similar results for different fill volumes and experiments. The dry layer resistance can be halved by LyoCoN from 87,732 m/s to 43,853 m/s and the variance is reduced by 90% from 33,526 m/s to 3168 m/s.

Finally, the model is validated for the primary drying of different freezing steps for accuracy and precision. The largest deviation between the simulation and experiment occurs with a freezing method ramp of 0.1 K/min. Here, an endpoint of $4.6 \pm 0.5\text{ h}$ is calculated and experimentally determined at $2.3 \pm 0.2\text{ h}$. For LyoCoN $-2\text{ }^{\circ}\text{C}$, a primary drying endpoint is calculated at $3.4 \pm 0.05\text{ h}$, for LyoCoN $-4\text{ }^{\circ}\text{C}$ at $3.4 \pm 0.05\text{ h}$, and for LyoCoN $-8\text{ }^{\circ}\text{C}$ at $3.3 \pm 0.07\text{ h}$. Experimentally, the endpoints here are $3.05 \pm 0.05\text{ h}$ (LyoCoN $-2\text{ }^{\circ}\text{C}$ and $-4\text{ }^{\circ}\text{C}$) and $2.9 \pm 0.1\text{ h}$, respectively. Controlled nucleation allows the simulation to describe the experiment, much more accurately reducing the deviation between them from factor 2 for shelf-ramped freezing to +8% using LyoCoN. A similar result is shown for a filling volume of 2 mL. The freezing methods without controlled nucleation display a clear deviation between the experiment and simulation. Ramp rates of 0.1 K/min calculate the end at $7 \pm 0.4\text{ h}$ (experiment: $5.35 \pm 0.15\text{ h}$), ramps of 2 K/min at $6.6 \pm 0.5\text{ h}$ (experiment: $5.65 \pm 0.65\text{ h}$), holding $0\text{ }^{\circ}\text{C}$ at $6.2 \pm 0.4\text{ h}$ (experiment: $5.4 \pm 1\text{ h}$) and holding at $-5\text{ }^{\circ}\text{C}$ at $6.6 \pm 0.35\text{ h}$ (experiment: $4.9 \pm 0.7\text{ h}$). The best results regarding the primary drying endpoint are obtained when freezing with LyoCoN $-2\text{ }^{\circ}\text{C}$ and precooled to $-45\text{ }^{\circ}\text{C}$. The calculated dryings are finished at $6.1 \pm 0.5\text{ h}$ and $6.1 \pm 0.3\text{ h}$, respectively, while the experiments are finished after $5.8 \pm 0.3\text{ h}$ and $6.2 \pm 0.55\text{ h}$, respectively. LyoCoN reduces the deviation between the experiment and simulation from 32% to 0.2%. Similar conclusions can be drawn for the middle vial. At a 1 mL filling volume, shelf-ramped freezing again shows the highest difference (simulation: $6 \pm 0.7\text{ h}$, experiment: $3.25 \pm 0.7\text{ h}$). LyoCoN reduces the variance from 84.6% to 7%. With a filling volume of 2 mL, LyoCoN $-2\text{ }^{\circ}\text{C}$ and precooling to $-45\text{ }^{\circ}\text{C}$ also show the best agreement for center vials reducing the relative difference from 25% to 0.12%.

Next, the model was validated for the primary drying product temperature. The largest deviation of the experimental product temperature could be described in the shelf-controlled freezing without a holding step. For the edge vials, a product temperature of $-21.9 \pm 1.8\text{ }^{\circ}\text{C}$ on average is calculated, but the experimental product temperature in

primary drying reaches only -32 ± 2 °C. The center vial reaches a lower average product temperature of -24.5 ± 2 °C than the edge vial in the simulation. However, this value is again higher than the experimentally determined one of -34 °C ± 2 °C. This high difference between the experiment and simulation can be decreased with the usage of LyoCoN. In the edge vial, the average calculated temperature is -32.2 ± 0.7 °C (experiment: -32.1 ± 2 °C) and the center vial is -34.1 ± 0.5 °C (experiment: -33.9 ± 2 °C). The simulated results of LyoCoN -8 °C experiments only deviate 0.31% for the edge and 0.59% for the center vial while the deviations increase drastically for shelf-ramped freezing up to 31.56% for the edge and 27.94 % for the center vial.

Controlled nucleation (LyoCoN) allows the control of the nucleation temperature of all vials during the freezing step, thus eliminating a main source of intra- and inter-batch heterogeneity by establishing a reproducible freezing process. Since the freezing behavior is adjusted in all vials, the determined R_p is more representable for the whole batch, increasing the simulation accuracy and precision. This kind of process control is demanded under the regulatory demanded QbD approach; therefore, a mechanism for controlled nucleation like LyoCoN should be incorporated into the freeze-drying cycle.

In combination, the physicochemical model and PAT tools can be used to achieve advanced process control (APC). The recommended PAT tools are shown in Table 6.

Table 6. PAT tools and their recommendation for usage in process control (green—fully recommended, yellow—limited recommendation, and orange—more experience necessary) (extended from Juckers et al. [57]).

PAT Tool	Necessary Equipment	Objective	Rec.	Remarks
WTM	WTMplus sensor Transponder	Product temperature determination	Yellow	Major advantages over wired sensors but invasive
Comp. pressure	Pirani gauge Capacitive sensor	Pressure control	Green	Pressure control can be obtained by either sensor Pirani: gas-type-dependent Capacitive: gas-type-independent
		Primary drying endpoint	Green	Measures endpoint of the whole batch
MTM	Two-chamber freeze dryer with closable intermediate valve Analysis tool	Model parameter determination R_p	Green	Noninvasive online measurement, value valid until 2/3 of primary drying
		Primary drying endpoint	Green	Pressure rise can induce melt back if the recipe is too aggressive Optimized MTM for reduced measurement time
Heat flux	Heat flux sensor Datalogger Readout software	Nucleation temperature determination	Yellow	Only measurement possible; combination with controlled nucleation required
		Model parameter determination K_v	Orange	Value significantly underestimated; more experience must be gained
		Primary drying endpoint	Yellow	Value in good agreement with WTM but exact positioning necessary
Ice ruler	Ice ruler Camera Analysis tool	Primary drying endpoint	Green	Sublimated ice mass in good agreement with ice occupation Analysis algorithm required
LyoCoN	LyoCoN reservoir	Nucleation temperature	Green	Nucleation temperature and pressure have to be optimized for formulation

During the primary drying process, the product temperature and sublimation rate must be kept below a critical value at all times. The model can predict these values based on limited online measured or previously determined data and modify the process with model predictive control. The dry layer resistance R_p is determined by MTM online during a primary drying experiment with the product while the vial heat transfer coefficient K_v is determined by ice sublimation tests beforehand. The estimated work effort is 10 to 15 days and has to be determined once for the used vials and freeze dryer and can then be used in development for different products. The primary drying endpoint of the batch

is important to ensure maximum productivity while maintaining product quality. Here, the usage of comparative pressure and manometric temperature measurement is strongly recommended. One sensor of the two used in comparative pressure measurement is used to control the pressure in the drying chamber and the other runs along to determine the batch end point of primary drying. MTM is used to determine the dry layer resistance during primary drying and pass this data to the model to enable adjustment of the simulations with real-time data. It is further used as a complementary method for primary drying endpoint determination to comparative pressure measurement showing differences of 4% [48]. In the pilot scale, product temperatures continue to be measured with WTMplus so that product temperature data are available for model validation. Furthermore, the usage of a heat flow sensor and an ice ruler is recommended. The ice ruler shows promising results at the pilot scale for monitoring the sublimation rate to keep it under the critical value [57]. The heat flux sensor can be used to optimize the freezing step by measuring the heat flux during nucleation and then adjusting the shelf temperature accordingly. LyoCoN is used in both scales to keep the freezing step comparable and to control the timing of nucleation. It is important that nucleation of all vials is controlled; a shelf temperature range of -2 to -8 °C should be used and the samples should be equilibrated beforehand to achieve a similar supercooling level over the sample height. The APC concept is shown in Figure 23.

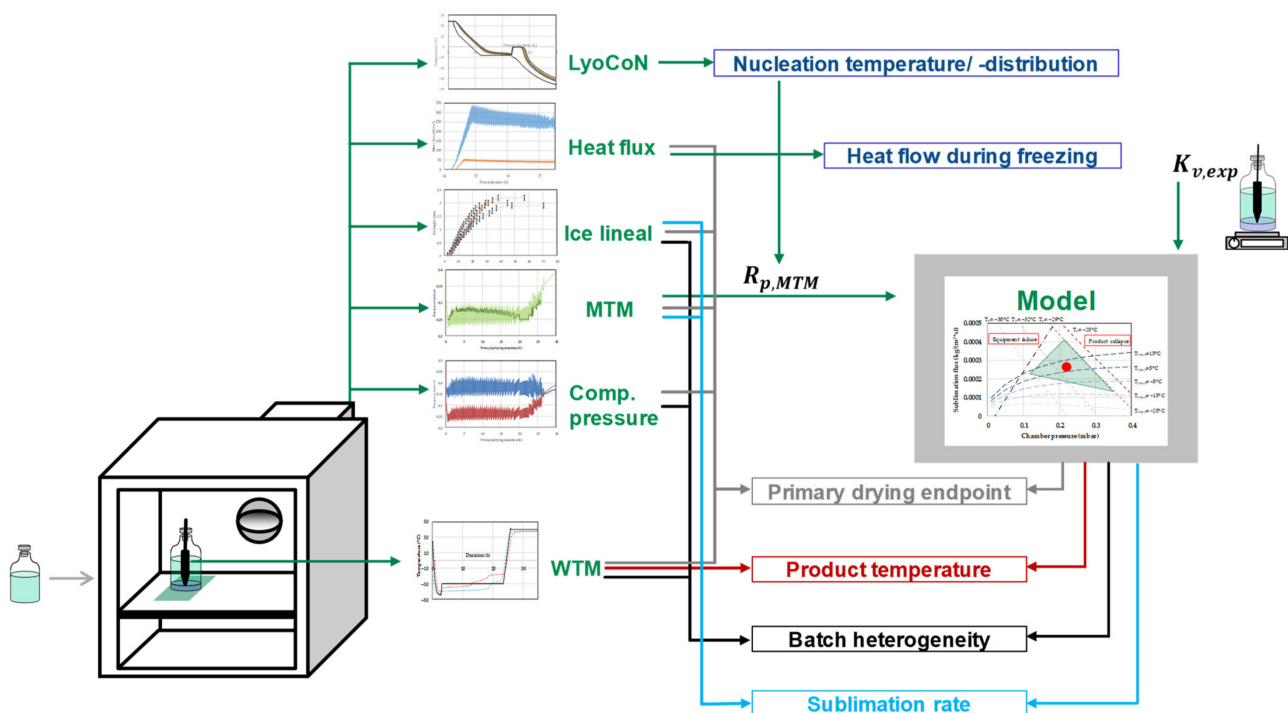


Figure 23. APC concept for lyophilization processes in vials.

The control of the nucleation temperature is crucial to obtain reliable and reproducible primary drying experiments and simulations as shown in Sections 5.4 and 5.5. It equalizes the temperature history of all vials in a batch and throughout all batches and is thus favorable inside the QbD concept. The simulation accuracy and precision of the product temperature drastically increases with controlled nucleation reducing the difference between the simulation and experiment from 31.56% to 0.31% with the same working effort. For optimal primary drying design and model predictive control, the nucleation temperature is strongly recommended to be controlled inside a PAT concept (see Table 6) and aggressive primary drying conditions should be used to achieve process efficiency while maintaining product safety.

Author Contributions: A.J. performed experiments, modeling and simulation and wrote this paper. P.K. and F.H. assisted with laboratory and piloting equipment as well as with expert knowledge regarding operations and objectives. J.S. was responsible for conception and supervision. All authors have read and agreed to the published version of the manuscript.

Funding: This research received no external funding.

Data Availability Statement: Data cannot be made publicly available.

Acknowledgments: We gratefully acknowledge the support of P. Knerr and F. Harms from Martin Christ Gefriertrocknungsanlagen GmbH for kindly providing the Epsilon 2-6D LSCplus as well as ongoing advice and support. The authors acknowledge support by Open Access Publishing Fund of Clausthal University of Technology.

Conflicts of Interest: The authors declare no conflict of interest. The company had no role in the design of the study; in the collection, analysis, or interpretation of data; or in the decision to publish the results.

References

- Ohtake, S.; Izutsu, K.; Lechuga Ballesteros, D. (Eds.) *Drying Technologies for Biotechnology and Pharmaceutical Applications*; Wiley-VCH: Weinheim, Germany, 2020; ISBN 9783527341122.
- Difranco, N. Lyophilization of Pharmaceuticals: An Overview. Lubrizol CDMO. 8 October 2019. Available online: <https://lubrizolcdmo.com/blog/lyophilization-of-pharmaceuticals-an-overview/> (accessed on 3 December 2020).
- Price, E. What is Driving the Growing Demand for Lyophilization? PCI Synthesis. 15 August 2019. Available online: <https://www.pcisynthesis.com/what-is-driving-the-growing-demand-for-lyophilization/> (accessed on 3 December 2020).
- Tang, X.; Pikal, M.J. Design of freeze-drying processes for pharmaceuticals: Practical advice. *Pharm. Res.* **2004**, *21*, 191–200. [[CrossRef](#)] [[PubMed](#)]
- Franks, F.; Auffret, T. *Freeze-Drying of Pharmaceuticals and Biopharmaceuticals*; RSC Publishing: Cambridge, UK, 2007.
- Walters, R.H.; Bhatnagar, B.; Tchessalov, S.; Izutsu, K.; Tsumoto, K.; Ohtake, S. Next generation drying technologies for pharmaceutical applications. *J. Pharm. Sci.* **2014**, *103*, 2673–2695. [[CrossRef](#)] [[PubMed](#)]
- Assegehegn, G.; La Brito-de Fuente, E.; Franco, J.M.; Gallegos, C. The Importance of Understanding the Freezing Step and Its Impact on Freeze-Drying Process Performance. *J. Pharm. Sci.* **2019**, *108*, 1378–1395. [[CrossRef](#)] [[PubMed](#)]
- Greiff, D. Development of cycles for lyophilization. *Dev. Biol. Stand.* **1992**, *74*, 85–92.
- Mirasol, F. Lyophilization Presents Complex Challenges. *BioPharm Int.* **2020**, *33*, 22–24.
- EMA. ICH Guideline Q8 (R2) on Pharmaceutical Development. Available online: https://www.ema.europa.eu/en/documents/scientific-guideline/international-conference-harmonisation-technical-requirements-registration-pharmaceuticals-human-use_en-11.pdf (accessed on 24 June 2022).
- FDA. PAT—A Framework for Innovative Pharmaceutical Development, Manufacturing, and Quality Assurance. FDA. 11 June 2020. Available online: <https://www.fda.gov/regulatory-information/search-fda-guidance-documents/pat-framework-innovative-pharmaceutical-development-manufacturing-and-quality-assurance> (accessed on 15 February 2021).
- Thomas, F. Changing Perceptions: An Understanding of Lyophilization Advancements. *Pharm. Technol.* **2019**, *43*, 32–34.
- Arsiccio, A.; Pisano, R. Application of the Quality by Design Approach to the Freezing Step of Freeze-Drying: Building the Design Space. *J. Pharm. Sci.* **2018**, *107*, 1586–1596. [[CrossRef](#)]
- Arsiccio, A.; McCarty, J.; Pisano, R.; Shea, J.-E. Heightened Cold-Denaturation of Proteins at the Ice-Water Interface. *J. Am. Chem. Soc.* **2020**, *142*, 5722–5730. [[CrossRef](#)]
- Arsiccio, A.; Marengo, L.; Pisano, R. A model-based approach for the rational design of the freeze-thawing of a protein-based formulation. *Pharm. Dev. Technol.* **2020**, *25*, 823–831. [[CrossRef](#)]
- Arsiccio, A.; Giorsello, P.; Marengo, L.; Pisano, R. Considerations on Protein Stability during Freezing and Its Impact on the Freeze-Drying Cycle: A Design Space Approach. *J. Pharm. Sci.* **2020**, *109*, 464–475. [[CrossRef](#)]
- Helgers, H.; Schmidt, A.; Lohmann, L.J.; Vetter, F.L.; Juckers, A.; Jensch, C.; Mouellef, M.; Zobel-Roos, S.; Strube, J. Towards Autonomous Operation by Advanced Process Control—Process Analytical Technology for Continuous Biologics Antibody Manufacturing. *Processes* **2021**, *9*, 172. [[CrossRef](#)]
- Pikal, M.J.; Rambhatla, S.; Ramot, R. The impact of the freezing stage in lyophilization: Effects of the ice nucleation temperature on process design and product quality. *Am. Pharmaceut. Rev.* **2002**, *5*, 48.
- Jennings, T. The Freezing Process. In *Lyophilization: Introduction and Basic Principles*; Interpharm Press: Englewood, CO, USA, 1999.
- Pisano, R.; Capozzi, L.C. Prediction of product morphology of lyophilized drugs in the case of Vacuum Induced Surface Freezing. *Chem. Eng. Res. Des.* **2017**, *125*, 119–129. [[CrossRef](#)]
- Arsiccio, A.; Pisano, R. The Ice-Water Interface and Protein Stability: A Review. *J. Pharm. Sci.* **2020**, *109*, 2116–2130. [[CrossRef](#)]
- Nail, S.L.; Jiang, S.; Chongprasert, S.; Knopp, S.A. Fundamentals of freeze-drying. In *Development and Manufacture of Protein Pharmaceuticals*; Springer: New York, NY, USA, 2002.

23. Kasper, J.C.; Friess, W. The freezing step in lyophilization: Physico-chemical fundamentals, freezing methods and consequences on process performance and quality attributes of biopharmaceuticals. *Eur. J. Pharm. Biopharm.* **2011**, *78*, 248–263. [[CrossRef](#)]
24. Rambhatla, S.; Ramot, R.; Bhugra, C.; Pikal, M.J. Heat and mass transfer scale-up issues during freeze drying: II. Control and characterization of the degree of supercooling. *AAPS PharmSciTech* **2004**, *5*, e58. [[CrossRef](#)]
25. Liu, J. Physical characterization of pharmaceutical formulations in frozen and freeze-dried solid states: Techniques and applications in freeze-drying development. *Pharm. Dev. Technol.* **2006**, *11*, 3–28. [[CrossRef](#)]
26. Searles, J.A. Freezing and annealing phenomena in lyophilization. In *Freeze-Drying/Lyophilization of Pharmaceutical and Biological Products*; CRC Press: Boca Raton, FL, USA, 2004.
27. Dalvi-Isfahan, M.; Hamdami, N.; Xanthakis, E.; Le-Bail, A. Review on the control of ice nucleation by ultrasound waves, electric and magnetic fields. *J. Food Eng.* **2017**, *195*, 222–234. [[CrossRef](#)]
28. Petzold, G.; Aguilera, J.M. Ice Morphology: Fundamentals and Technological Applications in Foods. *Food Biophys.* **2009**, *4*, 378–396. [[CrossRef](#)]
29. Akyurt, M.; Zaki, G.; Habeebullah, B. Freezing phenomena in ice–water systems. *Energy Convers. Manag.* **2002**, *43*, 1773–1789. [[CrossRef](#)]
30. Matsumoto, M.; Saito, S.; Ohmine, I. Molecular dynamics simulation of the ice nucleation and growth process leading to water freezing. *Nature* **2002**, *416*, 409–413. [[CrossRef](#)] [[PubMed](#)]
31. Jennings, T. The importance of process water. In *Lyophilization: Introduction and Basic Principles*; Interpharm Press: Englewood, CO, USA, 1999.
32. Wilson, P.W.; Heneghan, A.F.; Haymet, A.D.J. Ice nucleation in nature: Supercooling point (SCP) measurements and the role of heterogeneous nucleation. *Cryobiology* **2003**, *46*, 88–98. [[CrossRef](#)] [[PubMed](#)]
33. Blond, G. Velocity of linear crystallization of ice in macromolecular systems. *Cryobiology* **1988**, *25*, 61–66. [[CrossRef](#)] [[PubMed](#)]
34. Searles, J.A.; Carpenter, J.F.; Randolph, T.W. The ice nucleation temperature determines the primary drying rate of lyophilization for samples frozen on a temperature-controlled shelf. *J. Pharm. Sci.* **2001**, *90*, 860–871. [[CrossRef](#)] [[PubMed](#)]
35. Liu, J.; Viverette, T.; Virgin, M.; Anderson, M.; Paresh, D. A study of the impact of freezing on the lyophilization of a concentrated formulation with a high fill depth. *Pharm. Dev. Technol.* **2005**, *10*, 261–272. [[CrossRef](#)] [[PubMed](#)]
36. Hatley, R.H.; Mant, A. Determination of the unfrozen water content of maximally freeze-concentrated carbohydrate solutions. *Int. J. Biol. Macromol.* **1993**, *15*, 227–232. [[CrossRef](#)]
37. Pikal, M.J.; Shah, S.; Senior, D.; Lang, J.E. Physical chemistry of freeze-drying: Measurement of sublimation rates for frozen aqueous solutions by a microbalance technique. *J. Pharm. Sci.* **1983**, *72*, 635–650. [[CrossRef](#)]
38. Shibkov, A.A.; Golovin, Y.; Zheltov, M.A.; Korolev, A.A.; Leonov, A.A. Morphology diagram of nonequilibrium patterns of ice crystals growing in supercooled water. *Phys. A Stat. Mech. Its Appl.* **2003**, *319*, 65–79. [[CrossRef](#)]
39. Cameron, P. *Good Pharmaceutical Freeze-Drying Practice*; Interpharm Press Inc.: Englewood, CO, USA, 1997.
40. Blond, G.; Simatos, D.; Catté, M.; Dussap, C.G.; Gros, J.B. Modeling of the water-sucrose state diagram below 0 °C. *Carbohydr. Res.* **1997**, *298*, 139–145. [[CrossRef](#)]
41. Kett, V.; McMahan, D.; Ward, K. Thermoanalytical techniques for the investigation of the freeze drying process and freeze-dried products. *Curr. Pharm. Biotechnol.* **2005**, *6*, 239–250. [[CrossRef](#)]
42. Andrieu, J.; Vessot, S. A review on experimental determination and optimization of physical quality factors during pharmaceuticals freeze-drying cycles. *Dry. Technol.* **2018**, *36*, 129–145. [[CrossRef](#)]
43. Her, L.M.; Nail, S.L. Measurement of glass transition temperatures of freeze-concentrated solutes by differential scanning calorimetry. *Pharm. Res.* **1994**, *11*, 54–59. [[CrossRef](#)]
44. Ma, X.; Wang, D.Q.; Bouffard, R.; MacKenzie, A. Characterization of murine monoclonal antibody to tumor necrosis factor (TNF-MAb) formulation for freeze-drying cycle development. *Pharm. Res.* **2001**, *18*, 196–202. [[CrossRef](#)]
45. Schawe, J. A quantitative DSC analysis of the metastable phase behavior of the sucrose–water system. *Thermochim. Acta* **2006**, *451*, 115–125. [[CrossRef](#)]
46. Sacha, G.A.; Nail, S.L. Thermal analysis of frozen solutions: Multiple glass transitions in amorphous systems. *J. Pharm. Sci.* **2009**, *98*, 3397–3405. [[CrossRef](#)]
47. Ward, K.R.; Matejutschek, P. The use of microscopy, thermal analysis, and impedance measurements to establish critical formulation parameters for freeze-drying cycle development. In *Freeze-Drying/Lyophilization of Pharmaceutical and Biological Products*; CRC Press: Boca Raton, FL, USA, 2010; p. 112.
48. Knopp, M.M.; Löbmann, K.; Elder, D.P.; Rades, T.; Holm, R. Recent advances and potential applications of modulated differential scanning calorimetry (mDSC) in drug development. *Eur. J. Pharm. Sci.* **2016**, *87*, 164–173. [[CrossRef](#)]
49. Passot, S.; Fonseca, F.; Alarcon-Lorca, M.; Rolland, D.; Marin, M. Physical characterisation of formulations for the development of two stable freeze-dried proteins during both dried and liquid storage. *Eur. J. Pharm. Biopharm.* **2005**, *60*, 335–348. [[CrossRef](#)]
50. Meister, E.; Gieseler, H. Freeze-dry microscopy of protein/sugar mixtures: Drying behavior, interpretation of collapse temperatures and a comparison to corresponding glass transition data. *J. Pharm. Sci.* **2009**, *98*, 3072–3087. [[CrossRef](#)]
51. Depaz, R.A.; Pansare, S.; Patel, S.M. Freeze-Drying Above the Glass Transition Temperature in Amorphous Protein Formulations While Maintaining Product Quality and Improving Process Efficiency. *J. Pharm. Sci.* **2016**, *105*, 40–49. [[CrossRef](#)]
52. Horn, J.; Friess, W. Detection of Collapse and Crystallization of Saccharide, Protein, and Mannitol Formulations by Optical Fibers in Lyophilization. *Front. Chem.* **2018**, *6*, 4. [[CrossRef](#)]

53. Pisano, R. Alternative Methods of Controlling Nucleation in Freeze Drying. In *Lyophilization of Pharmaceuticals and Biologicals*; Ward, K.R., Matejtschuk, P., Eds.; Springer: New York, NY, USA, 2019; pp. 79–111. ISBN 978-1-4939-8927-0.
54. Velardi, S.A.; Barresi, A.A. Development of simplified models for the freeze-drying process and investigation of the optimal operating conditions. *Chem. Eng. Res. Des.* **2008**, *86*, 9–22. [[CrossRef](#)]
55. Juckers, A.; Knerr, P.; Harms, F.; Strube, J. Advanced Process Analytical Technology in Combination with Process Modeling for Endpoint and Model Parameter Determination in Lyophilization Process Design and Optimization. *Processes* **2021**, *9*, 1600. [[CrossRef](#)]
56. Juckers, A.; Knerr, P.; Harms, F.; Strube, J. Model-Based Product Temperature and Endpoint Determination in Primary Drying of Lyophilization Processes. *Pharmaceutics* **2022**, *14*, 809. [[CrossRef](#)] [[PubMed](#)]
57. Juckers, A.; Knerr, P.; Harms, F.; Strube, J. Emerging PAT for Freeze-Drying Processes for Advanced Process Control. *Processes* **2022**, *10*, 2059. [[CrossRef](#)]

Disclaimer/Publisher’s Note: The statements, opinions and data contained in all publications are solely those of the individual author(s) and contributor(s) and not of MDPI and/or the editor(s). MDPI and/or the editor(s) disclaim responsibility for any injury to people or property resulting from any ideas, methods, instructions or products referred to in the content.